Volume 6, Issue 12 – July – December – 2022

ECORFAN

Journal - Taiwan

ISSN-On line 2524-2121

ECORFAN®

ECORFAN Journal-Taiwan, Volume 6, Issue 12, December 2022, is a journal edited semestral by ECORFAN. Taiwan, Taipei. YongHe district, Zhong Xin, Street 69. Postcode: 23445. WEB: www.ecorfan.org/taiwan/journal@ecorfan.org. Editor in Chief: VARGAS-DELGADO, Oscar. PhD. ISSN: 2524-2121. Responsible for the latest update of this number ECORFAN Computer Unit. ESCAMILLA-BOUCHÁN, Imelda. PhD, LUNA-SOTO, Vladimir. PhD, last updated December 31, 2022.

ECORFAN Journal-Taiwan

Definition of Journal

Scientific Objectives

Support the international scientific community in its written production Science, Technology and Innovation in the Field of Physical Sciences Mathematics and Earth sciences, in Subdisciplines of optical astronomy, optical characterization, optical encoder, experimental research, planetary magnetic fields, ultraviolet radiation, lasers, algorithms and optical waves.

ECORFAN-Mexico, S. C. is a Scientific and Technological Company in contribution to the Human Resource training focused on the continuity in the critical analysis of International Research and is attached to CONACYT-RENIECYT number 1702902, its commitment is to disseminate research and contributions of the International Scientific Community, academic institutions, agencies and entities of the public and private sectors and contribute to the linking of researchers who carry out scientific activities, technological developments and training of specialized human resources with governments, companies and social organizations.

Encourage the interlocution of the International Scientific Community with other Study Centers in Mexico and abroad and promote a wide incorporation of academics, specialists and researchers to the publication in Science Structures of Autonomous Universities - State Public Universities - Federal IES - Polytechnic Universities - Technological Universities - Federal Technological Institutes - Normal Schools - Decentralized Technological Institutes - Intercultural Universities - S & T Councils - CONACYT Research Centers.

Scope, Coverage and Audience

ECORFAN Journal- Taiwan is a Journal edited by ECORFAN-Mexico, S. C. in its Holding with repository in Taiwan, is a scientific publication arbitrated and indexed with semester periods. It supports a wide range of contents that are evaluated by academic peers by the Double-Blind method, around subjects related to the theory and practice of optical astronomy, optical characterization, optical encoder, experimental research, planetary magnetic fields, ultraviolet radiation, lasers, algorithms and optical waves with diverse approaches and perspectives , That contribute to the diffusion of the development of Science Technology and Innovation that allow the arguments related to the decision making and influence in the formulation of international policies in the Field of Physical Sciences Mathematics and Earth sciences. The editorial horizon of ECORFAN-Mexico® extends beyond the academy and integrates other segments of research and analysis outside the scope, as long as they meet the requirements of rigorous argumentative and scientific, as well as addressing issues of general and current interest of the International Scientific Society.

Editorial Board

Arbitration Committee

Assignment of Rights

The sending of an Article to ECORFAN Journal-Taiwan emanates the commitment of the author not to submit it simultaneously to the consideration of other series publications for it must complement the Originality Format for its Article.

The authors sign the Authorization Format for their Article to be disseminated by means that ECORFAN-Mexico, S.C. In its Holding Taiwan considers pertinent for disclosure and diffusion of its Article its Rights of Work.

Declaration of Authorship

Indicate the Name of Author and Coauthors at most in the participation of the Article and indicate in extensive the Institutional Affiliation indicating the Department.

Identify the Name of Author and Coauthors at most with the CVU Scholarship Number-PNPC or SNI-CONACYT- Indicating the Researcher Level and their Google Scholar Profile to verify their Citation Level and H index.

Identify the Name of Author and Coauthors at most in the Science and Technology Profiles widely accepted by the International Scientific Community ORC ID - Researcher ID Thomson - arXiv Author ID - PubMed Author ID - Open ID respectively.

Indicate the contact for correspondence to the Author (Mail and Telephone) and indicate the Researcher who contributes as the first Author of the Article.

Plagiarism Detection

All Articles will be tested by plagiarism software PLAGSCAN if a plagiarism level is detected Positive will not be sent to arbitration and will be rescinded of the reception of the Article notifying the Authors responsible, claiming that academic plagiarism is criminalized in the Penal Code.

Arbitration Process

All Articles will be evaluated by academic peers by the Double Blind method, the Arbitration Approval is a requirement for the Editorial Board to make a final decision that will be final in all cases. MARVID® is a derivative brand of ECORFAN® specialized in providing the expert evaluators all of them with Doctorate degree and distinction of International Researchers in the respective Councils of Science and Technology the counterpart of CONACYT for the chapters of America-Europe-Asia- Africa and Oceania. The identification of the authorship should only appear on a first removable page, in order to ensure that the Arbitration process is anonymous and covers the following stages: Identification of the Journal with its author occupation rate - Identification of Authors and Coauthors - Detection of plagiarism PLAGSCAN - Review of Formats of Authorization and Originality-Allocation to the Editorial Board-Allocation of the pair of Expert Arbitrators-Notification of Arbitration -Declaration of observations to the Author-Verification of Article Modified for Editing-Publication.

Instructions for Scientific, Technological and Innovation Publication

Knowledge Area

The works must be unpublished and refer to topics of optical astronomy, optical characterization, optical encoder, experimental research, planetary magnetic fields, ultraviolet radiation, lasers, algorithms and optical waves and other topics related to Physical Sciences Mathematics and Earth sciences.

Presentation of the content

In the first article we present, *Rotational vibrations absorber analysis for damped oscillatory systems*, by VÁZQUEZ-GONZÁLEZ, Benjamín, JIMÉNEZ-RABIELA, Homero, RAMÍREZ-CRUZ, José Luis and GARCÍA-SEGURA, Pedro, with adscription in the Universidad Autónoma Metropolitana, in the next article we present, *Fiber optic coiling system prototype*, by RAMÍREZ-HERNÁNDEZ, Miguel Ángel, MEJÍA-BELTRÁN, Efraín, TALAVERA VELAZQUEZ, Dimas and GUTIÉRREZ-VILLALOBOS, José Marcelino, with adscription in the Centro de Investigaciones en Óptica, A.C. and Universidad Autónoma de Querétaro, in the next article we present, *Analysis of bathymetric surfaces for the determination of sediments in the inner basin of the port of Salina Cruz, Oaxaca*, by TREJO-LIEVANO DE LA ROSA, Carlo Saddam, AGUILAR-RAMIREZ, Ana María, DOMÍNGUEZ-GONZÁLEZ, Agustín and MOLINA-NAVARRO, Antonio, with adscription in the Instituto Oceanográfico del Golfo y Mar Caribe, in the last article we present, *Cost-effective automatic winder machine for optical fiber filament*, by GUTIERREZ-VILLALOBOS, José Marcelino, TALAVERA-VELÁZQUEZ, Dimas, MEJÍA-BELTRÁN, Efraín and RAMÍREZ-HERNÁNDEZ, Miguel Ángel, with adscription in the Universidad de Guanajuato and Universidad Autónoma de Querétaro.

Content

Article **ECORFAN Journal-Taiwan**
December 2022, Vol.6 No.12 1-9

Rotational vibrations absorber analysis for damped oscillatory systems

Análisis de un absorbedor de vibraciones tipo rotacional para sistemas con amortiguamiento

VÁZQUEZ-GONZÁLEZ, Benjamín†*, JIMÉNEZ-RABIELA, Homero, RAMÍREZ-CRUZ, José Luis and GARCÍA-SEGURA, Pedro

Universidad Autónoma Metropolitana, Unidad Azcapotzalco, División de Ciencias Básicas e Ingeniería, Departamento de Energía, Av. San Pablo 180 Colonia Reynosa Tamaulipas, Azcapotzalco C. P. 02200 Ciudad de México, México.

ID 1st Author: *Benjamín, Vázquez-González* / **ORC ID:** 0000-0002-9030-5662, **Researcher ID Thomson:** S-2417-2018, **CVU CONACYT ID:** 25749

ID 1st Co-author: *Homero, Jiménez-Rabiela* / **ORC ID:** 0000-0002-1549-0853, **Researcher ID Thomson:** S-2299-2018, **CVU CONACYT ID:** 123386

ID 2nd Co-author: *José Luis, Ramírez-Cruz* / **ORC ID:** 0000-0003-0762-2630, **Researcher ID Thomson:** G-3405-2019, **CVU CONACYT ID:** 921268

ID 3rd Co-author: *Pedro, García-Segura* / **ORC ID:** 0000-0003-4947-084X, **Researcher ID Thomson:** S-2360-2018, **CVU CONACYT ID:** 371233

DOI: 10.35429/EJT.2022.12.6.1.9 Received July 15, 2022; Accepted December 30, 2022

Abstract

The phenomenon of vibration absorption is an energy exchange mechanism, which can be used in mechanical engineering applications to solve problems of attenuation or reduction of high amplitudes that a moving body or system can reach. There are basically two types of vibration absorbers; passive and active. Active vibrations absorbers are composed of servomechanisms that are capable of modifying structural conditions, to produce a specific required performance. Passive vibrations absorbers are not made up of elements that directly modify the structure of the mechanical system as a whole, thus a passive system is designed to operate under conditions that will not change over time, however, active systems will require the addition of some type of external energy, passive systems do not consume extra energy and this makes them attractive from the point of view of their accessibility. In this work, the performance of a rotational-type passive vibration absorber for a primary system with harmonic excitation and viscous-type damping is studied.

Vibrations, Passive absorption, Viscous damping

Resumen

El fenómeno de la absorción de vibraciones es un mecanismo de intercambio de energético, el cual puede ser utilizado en aplicaciones de la ingeniería mecánica para resolver problemas de la atenuación o reducción de amplitudes elevadas que un cuerpo o sistema en movimiento puede alcanzar. Existen fundamentalmente dos tipos de absorbedores de vibraciones; los pasivos y los activos. Los absorbedores activos se componen de servomecanismos que son capaces de modificar condiciones estructurales, para producir un desempeño especifico requerido. Los absorbedores pasivos no se constituyen por elementos que modifiquen de forma directa la estructura del sistema mecánico en su conjunto, de esta forma un sistema pasivo está diseñado para operar bajo condiciones que no cambiarán en el tiempo, sin embargo, los sistemas activos requerirán de la adición de algún tipo de energía externa, los sistemas pasivos no consumen energía extra y esto los hace atractivos desde el punto de vista de su accesibilidad. En este trabajo se estudia el desempeño de un absorbedor de vibraciones pasivo tipo rotacional, para un sistema primario con excitación armónica y amortiguamiento de tipo viscoso.

Vibraciones, Absorción pasiva, Amortiguamiento viscoso

Citation: VÁZQUEZ-GONZÁLEZ, Benjamín, JIMÉNEZ-RABIELA, Homero, RAMÍREZ-CRUZ, José Luis and GARCÍA-SEGURA, Pedro. Rotational vibrations absorber analysis for damped oscillatory systems. ECORFAN Journal-Taiwan. 2022. 6-12:1-9.

* Author correspondence (E-mail: bvg@correo.azc.uam.mx)
† Researcher contributing as first author.

Introduction

In the disciplines of mechanical engineering science, the study of the vibration absorption phenomenon has been cultivated since its incipience, when Den Hartog managed to establish the direct interaction between the primary system and its absorber. Subsequent studies and developments have been directed towards expanding the absorption range of the absorber, these developments have led to the innovation of control techniques, an active absorber has as its fundamental reference a passive absorber, at the end of its performance the active absorber converges to passive. Novel techniques are presented in Cheung and Wong, work, where non-traditional designs of vibration absorbers are made, the technique presented in said work focuses on modifying the velocity amplitude of the primary system. For this reason, the analysis of passive vibration absorbers can be directed towards the development of active absorbers, reducing sophisticated control actions, which may require a long processing time, and may reduce their efficiency. Other techniques include damping modification along with tuning, Abdel-Hafiz and Hassaan they report results with these techniques. In this work, the analysis of a rotational type vibration absorber is carried out, for which the primary system is damped, Vázquez et. al. conducted a study for the undamped case.

The results obtained establish relations of amplitude of the vibration of the primary system in relation to the magnitude of the excitation force, likewise, it is determined that the absorption is defined by the tuning of the undamped frequency between the primary system and its absorber, in such a way that the damping does not have a direct influence, which allows modifying this parameter arbitrarily, however, the damping establishes a stable state regime.

The rotational absorber for a primary system with damping

The rotational absorber consists of a cylindrical mass m_2 which rolls without slipping on the body of the primary system m_1. This configuration establishes a geometric coupling, apart from the dynamic coupling defined by the spring k_2. The geometric coupling allows the absorber to be compact in the sense of being contained within the primary system. Figure 1 illustrates the above.

The damping, that is considered is present in the primary system and including its presence is necessary because the damping can produce phase shifts between the forcing action, as well as attenuation in the amplitude of the response of the primary system.

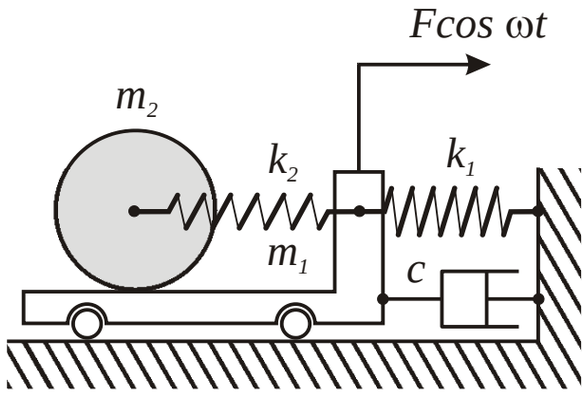

Figure 1 Rotational absorber m_2 coupled to the primary system m_1, due to elastic geometric and dynamic restriction

The rotational absorber is an interesting system to study, because it develops two types of movement that participate in the absorption of energy, these movements are the rotation of the primary system and the translation of the center of mass of the same absorber, unlike the single mass displacement absorber. The primary system consists of a spring-mass system, with viscous-type damping c, harmonic-type excitation with the frequency ω and magnitude F.

Dynamic equations of the rotational absorber

The dynamic equations of the system as a whole are determined using the Euler-Lagrange formulation, in Figure 2 the kinematic coordinates are illustrated.

The absorber has radius r and its displacement ratio is relative to the primary system motion.

Let *D* be the relative displacement between the center of mass of the primary system and its absorber, thus, in terms of the motion coordinates, it is true that,

ISSN 2524-2121

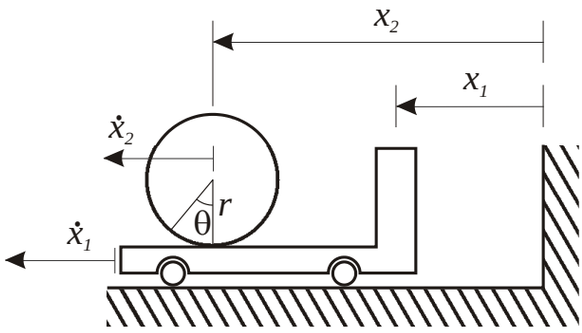

Figure 2 A scheme that identifies the kinematic coordinates of the primary system and its absorber

$$D = x_2 - x_1 \tag{1}$$

Figure 3 illustrates the relative displacement between both bodies.

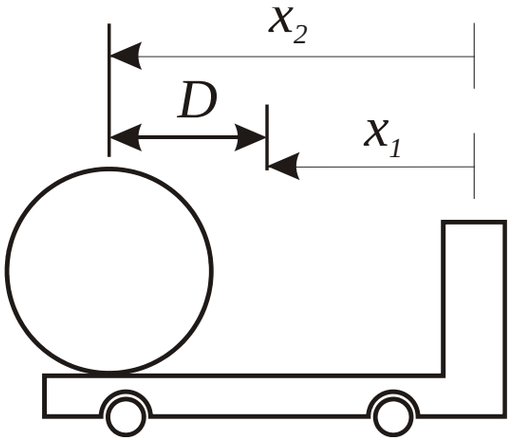

Figure 3 Determination of the relative displacement of the absorber in relation to the primary system

but,

$$D = r\theta = \mathrm{x}_2 - \mathrm{x}_1 \tag{2}$$

so,

$$\theta = \frac{\mathrm{x}_2 - \mathrm{x}_1}{r} \tag{3}$$

The variables in time are the position coordinates and the angular displacement, therefore, when differentiating equation (3) in time, its results,

$$\dot{\theta} = \frac{\dot{\mathrm{x}}_2 - \dot{\mathrm{x}}_1}{r} \tag{4}$$

The expression of the kinetic energy of the system requires determining the forms of the kinetic energy of each element of the system in motion, therefore, the total kinetic energy is,

$$T = \frac{1}{2}m_1\dot{x}_1^2 + \frac{1}{2}m_2\dot{x}_2^2 + \frac{1}{2}I\dot{\theta}^2 \tag{5}$$

and in terms of the displacement variables, it turns out

$$T = \frac{1}{2}m_1\dot{x}_1^2 + \frac{1}{2}m_2\dot{x}_2^2 + \frac{1}{2}I\left(\frac{\dot{x}_2 - \dot{x}_1}{r}\right)^2 \tag{6}$$

where I represents the moment of inertia of the cylinder or absorber,

$$I = \frac{1}{2}m_2r^2 \tag{7}$$

The potential energy of the system is manifested in the elastic elements, that is,

$$V = \frac{1}{2}k_1x_1^2 + \frac{1}{2}k_2(x_2 - x_1)^2 \tag{8}$$

The Lagrangian function L, is determined by the difference between the total kinetic and potential energy,

$$L = \frac{1}{2}m_1\dot{x}_1^2 + \frac{1}{2}m_2\dot{x}_2^2 + \frac{1}{4}m_2(\dot{x}_2 - \dot{x}_1)^2 - \frac{1}{2}k_1x_1^2 - \frac{1}{2}k_2(x_2 - x_1)^2 \tag{7}$$

The damper is a dissipative element of the system, it interacts directly with the primary system and its energy is quantified by the dissipation function,

$$\Delta = \frac{1}{2}\mathrm{c}\dot{\mathrm{x}}_1^2 \tag{8}$$

The Euler-Lagrange equations for this system, including the dissipative terms due to damping and with external excitation, are,

$$\frac{\mathrm{d}}{\mathrm{dt}}\left(\frac{\partial \mathrm{L}}{\partial \dot{\mathrm{x}}_1}\right) - \left(\frac{\partial \mathrm{L}}{\partial \mathrm{x}_1}\right) = \frac{\partial \Pi}{\partial \dot{x}_1} - \frac{\partial \Delta}{\partial \dot{x}_1} \tag{9}$$

$$\frac{\mathrm{d}}{\mathrm{dt}}\left(\frac{\partial \mathrm{L}}{\partial \dot{\mathrm{x}}_2}\right) - \left(\frac{\partial \mathrm{L}}{\partial \mathrm{x}_2}\right) = 0 \tag{10}$$

where,

$$\Pi = (\mathrm{F}\cos\omega\mathrm{t})\dot{\mathrm{x}}_1 \tag{11}$$

Expression (11) is known as the supplied power function, from this expression the excitation term is evaluated,

$$\frac{\partial \Pi}{\partial \dot{x}_1} = \mathrm{F}\cos\omega\mathrm{t} \tag{12}$$

By developing the partial and total derivatives of equations (9) and (10), together with the excitation expression, the following differential equations result,

$$\left(m_1 + \frac{1}{2}m_2\right)\ddot{x}_1 - \frac{1}{2}m_2\ddot{x}_1 + c\dot{x}_1 + (k_1 + k_2)x_1 - k_2x_2 = Fcos\omega t \tag{12}$$

ISSN 2524-2121

$$\frac{3}{2}m_2\ddot{x}_2 - \frac{1}{2}m_2\ddot{x}_1 + k_2x_2 - k_2x_1 = 0 \quad (13)$$

Finally, defining $M = m_1 + \frac{1}{2}m_2$, we have the following system of equations,

$$M\ddot{x}_1 - \frac{1}{2}m_2\ddot{x}_1 + c\dot{x}_1 + (k_1 + k_2)x_1 - k_2x_2 = Fcos\omega t \quad (14)$$

$$\frac{3}{2}m_2\ddot{x}_2 - \frac{1}{2}m_2\ddot{x}_1 + k_2x_2 - k_2x_1 = 0 \quad (15)$$

Determination of dynamic absorption conditions

The system of equations (14)-(15) corresponds to a coupled linear system of differential equations, to determine which performance conditions are met, the following set of solutions is proposed,

$$x_1(t) = X_{11}sen(\omega t) + X_{12}cos(\omega t) \quad (16)$$

$$x_2(t) = X_{21}sen(\omega t) + X_{22}cos(\omega t) \quad (17)$$

Where X_{11}, X_{12}, X_{21} and X_{22} they are associated with the amplitude of the movement that each element or body of the system can develop in time.

Differentiating in time equations (16)-(17) and substituting equations (14)-(15), the following set of four equations results,

$$-\omega^2 MX_{11} + \frac{1}{2}m_2\omega^2X_{21} - \omega cX_{12} + (k_1+k_2)X_{11} - k_2X_{21} = 0 \quad (18)$$

$$-\omega^2 MX_{12} + \frac{1}{2}m_2\omega^2X_{22} + \omega cX_{11} + (k_1+k_2)X_{12} - k_2X_{22} = F \quad (19)$$

$$-\omega^2\frac{3}{2}m_2X_{21} + \frac{1}{2}m_2\omega^2X_{11} + k_2X_{21} - k_2X_{12} = 0 \quad (20)$$

$$-\omega^2\frac{3}{2}m_2X_{22} + \frac{1}{2}m_2\omega^2X_{12} + k_2X_{22} - k_2X_{12} = 0 \quad (21)$$

The system of equations (18)-(21) can be written in matrix form for the four unknowns (X_{11}, X_{12}, X_{21}, X_{22}), the result is the following,

$$\begin{bmatrix} k_1+k_2-\omega^2M & -c\omega & \frac{1}{2}m_2\omega^2-k_2 & 0 \\ c\omega & k_1+k_2-\omega^2M & 0 & \frac{1}{2}m_2\omega^2-k_2 \\ \frac{1}{2}m_2\omega^2-k_2 & 0 & k_2-\frac{3}{2}m_2\omega^2 & 0 \\ 0 & \frac{1}{2}m_2\omega^2-k_2 & 0 & k_2-\frac{3}{2}m_2\omega^2 \end{bmatrix} \cdot \begin{bmatrix} X_{11} \\ X_{12} \\ X_{21} \\ X_{22} \end{bmatrix} = \begin{bmatrix} 0 \\ F \\ 0 \\ 0 \end{bmatrix} \quad (22)$$

From the system of equations (22), it is possible to determine dynamic conditions for absorption, which is reflected as the performance for which the resulting amplitude of the primary system is the smallest possible or null. In the process of searching for such conditions, it is first necessary to determine the expression of each of the components of the amplitude. The solutions for the system of equations of system (22) are presented below.

$$X_{11} = (36cm_2^2\omega^5 - 48ck_2m_2\omega^3 + 16ck_2^2\omega)\frac{F}{\Delta} \quad (23)$$

$$X_{12} = (a_1\omega^6 + b_2\omega^4 + c_2\omega^2 + f)\frac{F}{\Delta} \quad (24)$$

where,

$$a_1 = 6m_2^3 - 36Mm_2^2 \quad (25)$$

$$b_2 = 36k_1m_2^2 + 8k_2m_2^2 + 48Mk_2m_2 \quad (26)$$

$$c_2 = -(48k_1k_2m_2 + 16Mk_2^2 + 8k_2^2m_2) \quad (27)$$

$$f = 16k_1^2k_2^2 \quad (28)$$

$$X_{21} = (12cm_2^2\omega^5 - 32ck_2m_2\omega^3 + 16ck_2^2\omega)\frac{F}{\Delta} \quad (29)$$

$$X_{22} = (a_3\omega^6 + b_3\omega^4 + c_3\omega^2 + f)\frac{F}{\Delta} \quad (30)$$

where,

$$a_3 = 2m_2^3 - 12Mm_2^2 \quad (31)$$

$$b_3 = 12k_1m_2^2 + 32Mk_2m_2 \quad (32)$$

$$c_3 = -(32k_1k_2m_2 + 16Mk_2^2 + 8k_2^2m_2) \quad (33)$$

The determinant of the system of equations is the following,

$$\Delta = a\omega^8 + b\omega^6 + d\omega^4 + e\omega^2 + f \quad (34)$$

where in turn,

$$a = m_2^4 - 12Mm_2^3 + 36M^2m_2^2 \quad (35)$$

$$b = 12k_1m_2^3 + 4k_2m_2^3 - 72Mk_1m_2^2 - 16Mk_2m_2^2 - 48M^2k_2m_2 + 36c^2m_2^2 \quad (36)$$

$$d = 96Mk_1k_2m_2 + 16Mk_2^2m_2 - 48c^2k_2m_2 + 16k_1k_2m_2^2 + 16M^2k_2^2 + 36k_1^2m_2^2 + 4k_2^2m_2^2 \quad (37)$$

$$e = 16c^2k_2^2 - 16k_1k_2^2m_2 - 32Mk_1k_2^2 - 48k_1^2k_2m_2 \quad (38)$$

ISSN 2524-2121

The set of above expressions is very extensive as can be seen, however, it is possible to determine the parameters for the required performance.

It is sought that the amplitude of the primary system is as small as possible, which establishes that the amplitudes of the movement meet the following condition, $X_{11} = X_{12} = 0$.

From the numerator of equation (23) it can be seen that it can be reduced to the following expression,

$$X_{11} = (9m_2^2\omega^4 - 12k_2m_2\omega^2 + 4k_2^2)\omega c = 0 \quad (39)$$

since the frequency is not null because it is the movement parameter and the case in which damping is present is being analyzed, it is concluded that the required parameters are found in the expression,

$$9m_2^2\omega^4 - 12k_2m_2\omega^2 + 4k_2^2 = 0 \quad (40)$$

where does it come from,

$$\omega^2 = \frac{2k_2}{3m_2} \quad (41)$$

Equation (29), which corresponds to the second term of the amplitude of the primary system, can also provide information to determine the absorption parameters. Substituting expression (41) in equation (29) it is found that

$$X_{12} = X_{12}(\omega^2) = 0. \quad (42)$$

With which it is concluded that equations (23) and (24) are canceled for the tuning frequency (41), this allows choosing one of two design parameters for the vibration absorber, however, as observed, the damping c, is a parameter that does not participate in the absorption process, so it can be proposed arbitrarily. However, the damping c is present in the response of each element of the system, this is observed in the terms of the determinant (34), so the magnitude of the response is defined by the numerical value that it can reach.

A final stage of validation in determining the design parameters of the absorber consists of obtaining design parameters from equations (29) and (30).

However, reevaluating equation (41) in equations (29) and (30), results in the following,

$$X_{21} = X_{21}(\omega^2) = 0. \quad (43)$$

and

$$X_{22} = X_{22}(\omega^2) = 0. \quad (44)$$

With these results it is concluded that there is only one design parameter and it corresponds to equation (41).

Determination of response in time

To obtain a representation of the performance over time of the system and its absorber, the system of differential equations (14)–(15) is expressed in the state space representation, for which the following changes of variables are made,

$$\dot{x}_1 = \dot{y}_1, \dot{y}_1 = y_2, \dot{x}_2 = \dot{y}_3, \dot{y}_3 = y_4 \quad (45)$$

which allows us to write the system (14)-15 as,

$$\begin{bmatrix} \dot{y}_1 \\ \dot{y}_2 \\ \dot{y}_3 \\ \dot{y}_4 \end{bmatrix} = \begin{bmatrix} 0 & 1 & 0 & 0 \\ \frac{6k_1 + 4k_2}{d_1} & \frac{6c}{d_1} & -\frac{4k_2}{d_1} & 0 \\ 0 & 0 & 0 & 1 \\ \frac{2k_2 - 2k_1}{d_1} & -\frac{4Mk_2}{d_2} & \frac{2c}{d_1} & \frac{4Mk_2}{d_2} \end{bmatrix} \begin{bmatrix} y_1 \\ y_2 \\ y_3 \\ y_4 \end{bmatrix} + \begin{bmatrix} 0 \\ -\frac{6F\cos\omega t}{d_1} \\ 0 \\ -\frac{2F\cos\omega t}{d_1} \end{bmatrix} \quad (46)$$

where, $d_1 = m_2 - 6M$ and $d_2 = m_2(m_2 - 6M)$

The representation in the space of states allows to obtain answers in time, from numerical simulations.

Time responses of the primary system and its absorber

Simulation results are presented in the time response of the system from the state space representation. The simulations are performed in situations in which is tuned to the absorber for equation (41) and in its case different damping values, the above is the result of having determined that damping is a parameter that can be set arbitrarily, however, it is part of the system response. The values of force and frequency are arbitrary, however, they are significant, in the sense that a clear perception can be had about the effect that 15 N produces on a mass of 4 kg.

ISSN 2524-2121

The frequency has been chosen to be 5 rad/sec., which also allows us to clearly observe the shape of the response over time.

Table 1 shows the data for a very massive primary system in relation to its absorber, the tuning is not performed and an arbitrary viscous damping is considered.

m_1= 4 kg	m_2= 0.5 kg	k_1 = 100 N/m
k_2 = 300 N/m	F = 15 N	ω = 5 rad/s
c = 10 N·s/m		

Table 1 Parameters of the vibrating mechanical system corresponding to Figures 4 and 5

Figure 4 shows the time response of the primary system $x_1(t)$ for the data in Table 1. The magnitude of the amplitude is approximately $x_1(t)$ = 0.13 m, likewise, a uniform response is verified, according to the steady state. There is no tuning between both subsystems.

Figure 5 shows the time response of the secondary system $x_2(t)$ for the parameters in Table 1, in which the tuning condition is not considered. The amplitude of the absorber reaches approximately $x_2(t)$ = 0.14 m.

Table 2 shows the set of parameters for the previous experiment, in this case there is the tuning condition between the primary and secondary systems.

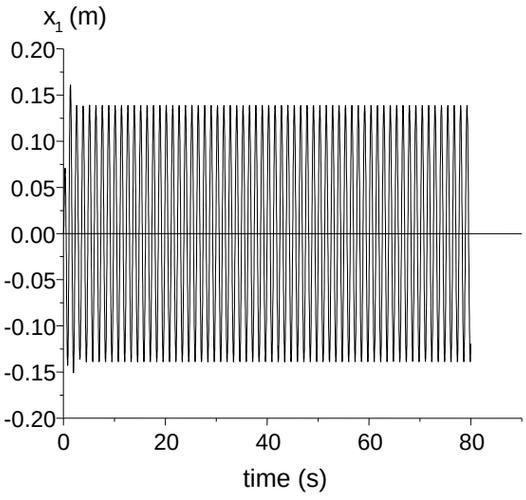

Figure 4 Time response of the primary system for the parameters in Table 1

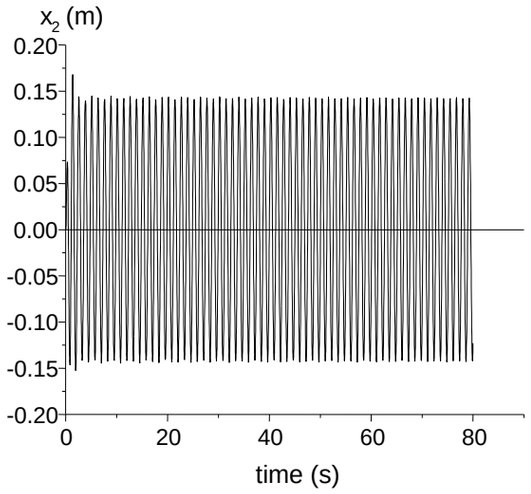

Figure 5 Response in time of the secondary system for the parameters in Table 1

m_1= 4 kg	m_2= 0.5 kg	k_1 = 100 N/m
k_2 =18.75N/m	F = 15 N	ω = 5 rad/s
c = 10 N·s/m		

Table 2 Parameters of the vibrating mechanical system corresponding to Figures 6 and 7

Figure 6 shows the time response of the primary system in tuning with its absorber, in accordance with the data in Table 2. The amplitude of the primary system reaches a value $x_1(t)$ = 0.065 m in the steady state, in relation to Figure 4, which corresponds to the primary system without tuning, a reduction of close to 50% is observed.

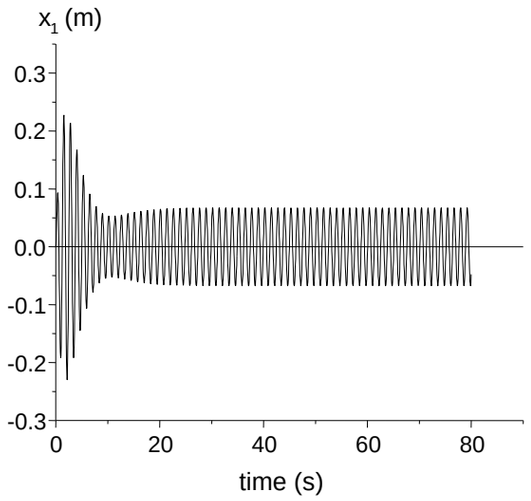

Figure 6 Time response of the primary system for the parameters in Table 2

ISSN 2524-2121

Figure 7 shows the time response of the absorber for the parameters in Table 2, the developed amplitude reaches $x_2(t) = 2.24$ m, this magnitude corresponds to a hypothetical case, in according to the proposed data, however, the effect of absorption can be observed, which requires a high amplitude to absorb and release the mechanical energy transferred from the primary to the secondary system.

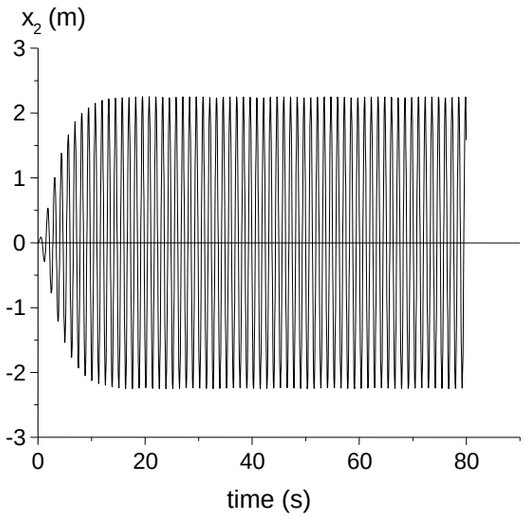

Figure 7 Time response of the primary system for the parameters in Table 2

Table 3 shows the same parameters as Table 2, with the exception that the damping value has been modified, remembering that this parameter can be modified arbitrarily, in this case its numerical value has been doubled and it follows keeping the tuning.

m_1= 4 kg	m_2=0.5 kg	k_1 = 100 N/m
k_2 =18.75N/m	F = 15 N	ω = 5 rad/s
c = 20 N·s/m		

Table 3. *Parameters of the vibrating mechanical system corresponding to Figures 8 and 9.*

Figure 8 shows the response in time for the primary system for the data in Table 3, in this case the tuning of the primary system with its absorber is preserved, but the damping value has been increased twice in relation to Table 2. A steady state amplitude of approximately $x_1(t) = 0.062$ m is identified, which means a small decrease in relation to the previous experiment.

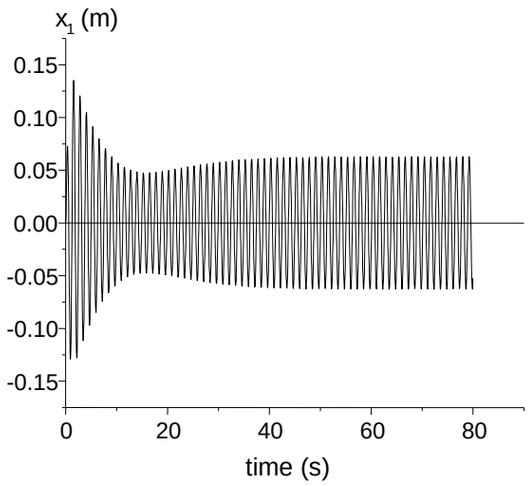

Figure 8 Time response of the primary system for the parameters in Table 3

Figure 9 shows the time response of the absorber for the data in Table 3. The amplitude recorded in the stable state reaches a value of $x_2(t) = 2.089$ m, which represents a very small value in the decrease amplitude in relation to the parameters in Table 2.

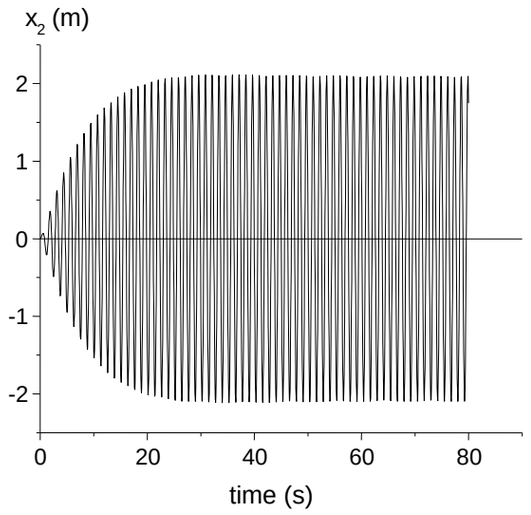

Figure 9 Time response of the secondary system for the parameters in Table 3

Table 4 shows the parameters in which the mass of the absorber has doubled in relation to the previous experiments, the value of viscous damping c has decreased by half, tuning is considered, for this reason, we have a value of k_2 different from the previous ones.

m_1= 4 kg	m_2=1 kg	k_1 = 100 N/m
k_2 =37.5N/m	F = 15 N	ω = 5 rad/s
c = 10 N·s/m		

Table 4 Parameters of the vibrating mechanical system corresponding to Figures 10 and 11

ISSN 2524-2121

Figure 10 shows the graph of the development over time of the primary system. The amplitude in the stable state reports a magnitude of $x_1(t) = 0.061$ m, tuning is present and although the damping is the same as that of the parameters in Table 3, the mass of the absorber has increased, the amplitudes, between Figures 8 and 10 are very similar, however, it can be seen in Figure 11, that the amplitude of the absorber has decreased in a proportion close to half, this is due to the increase in energy consumption to put in motion a greater mass, the measured amplitude has an approximate value of $x_2(t) = 1.09$ m. Table 5 shows the parameters for the last experiment, the mass of the absorber has doubled, as well as the viscous damping c, in relation to the parameters in Table 4.

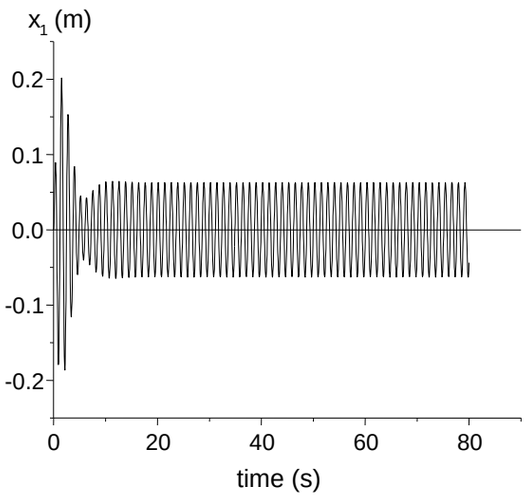

Figure 10 Time response of the primary system for the parameters in Table 4

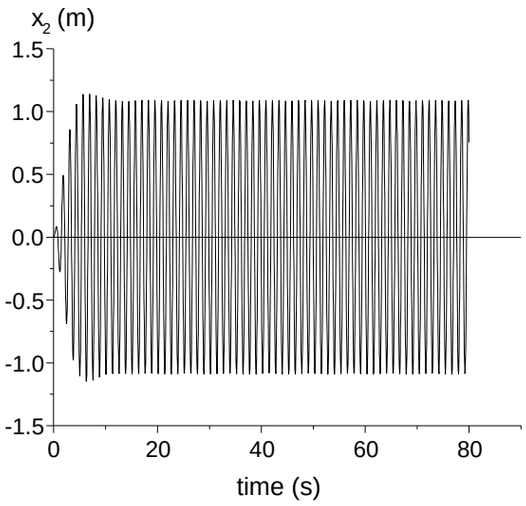

Figure 11 Time response of the secondary system for the parameters in Table 4

Tuning is considered in the experiment. It should be noted that in the cases of tuning, a different value is obtained when the value of the absorber mass is modified, which produces an effect of variable elastic stiffness.

m_1= 4 kg	m_2=2 kg	k_1 = 100 N/m
k_2 = 75 N/m	F = 15 N	ω = 5 rad/s
c = 20 N·s/m		

Table 5 Parameters of the vibrating mechanical system corresponding to Figures 12 and 13

Figure 12 shows a greater attenuation of the amplitude of the movement of the primary system, $x_1(t) = 0.053$ m, in relation to Figure 10.

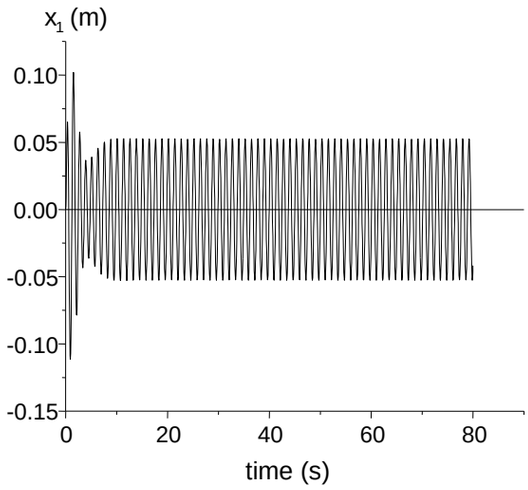

Figure 12 Time response of the primary system for the parameters in Table 5

Figure 13 shows the time response of the absorber, it is observed that the joint effect of increasing the mass of the absorber and increasing the damping, under the tuning condition and this produces a reduction in the amplitude of the primary system and significantly in that of the secondary, $x_2(t) = 0.049$ m, again a value close to half the response of the secondary system in relation to the parameters in Table 4.

ISSN 2524-2121

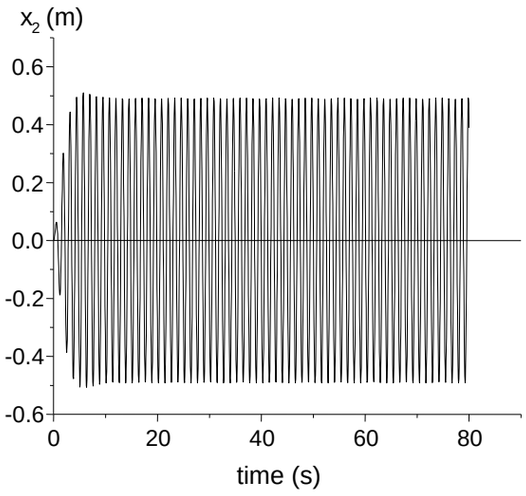

Figure 13 Response in time of the secondary system for the parameters in Table 5

Acknowledgement

The authors appreciate the institutional support of the Universidad Autónoma Metropolitana and the Azcapotzalco Campus, in particular the Division of Basic Sciences and Engineering and the Department of Energy.

Conclusions

Vibration absorption is a complex phenomenon of mechanical systems, its implementation in mechanical engineering requires the study of mechanical energy transfer phenomena. Knowing the effects of modifying some parameters is important to achieve efficient device design and development, even more so when simple devices are implemented in complex performances. In this work, the analysis of a rotational type vibration absorber has been developed for the case of a primary system with viscous type damping. The reported results present the possibility of openly choosing the damping value, which induces the behavior of the stable state in both bodies of the system as a whole and, in turn, knowing in advance the tuning condition, efficient results are obtained in the sense to reduce the amplitude of both the primary and secondary systems. The rotational absorber for a forced system with viscous damping allows adjustments in the parameters in such a way that the attenuation of the amplitude of the primary system, as well as of the secondary, is achieved.

References

Den Hartog J P. Mechanical vibrations. Dover Publications Inc; 1985.

Mohammed Abdel-Hafiz and Galal Ali Hassaan. (2015) Tuning Condition Modification of Damped and Un-damped Adaptive Vibration Absorber. International Journal of Computer Techniques, Volume 2, Issue 2, 2015,170-175. http://www.ijctjournal.org/Volume2/Issue2/IJCT-V2I2P28.pdf

Vázquez González Benjamín, Jiménez Rabiela Homero, Ramírez Cruz José Luis, (2020) Design of a rotational type vibration absorber. Journal of Mechanical Engineering, ECORFAN-Spain. June 2020, Vol.4, No.13 16-22. DOI: 10.35429/JME.2020.13.4.16.22.

Y. L. Cheung and W. O. Wong. (2009) Design of a non-traditional dynamic vibration absorber (L). J. Acoust. Soc. Am. 126 (2), August 2009, 564-567. DOI: 10.1121/1.3158917.

ISSN 2524-2121

Article **ECORFAN Journal-Taiwan**
December 2022, Vol.6 No.12 10-15

Fiber optic coiling system prototype

Prototipo de sistema enrollador de fibra óptica

RAMÍREZ-HERNÁNDEZ, Miguel Ángel†´, MEJÍA-BELTRÁN, Efraín*´, TALAVERA VELAZQUEZ, Dimas´´ and GUTIÉRREZ-VILLALOBOS, José Marcelino´´

´*Centro de Investigaciones en Óptica, A.C., CONACYT, León, Gto., México*
´´*Universidad Autónoma de Querétaro, Querétaro, Qro., México*

ID 1st Author: *Miguel Ángel, Ramírez-Hernández* / **ORC ID:** 0000-0002-6093-090X, **CVU CONACYT ID:** 742457

ID 1st Co-author: *Efraín, Mejía-Beltrán* / **ORC ID:** 0000-0001-8960-6604, **CVU CONACYT ID:** 20998

ID 2nd Co-author: *Dimas, Talavera-Velazquez* / **ORC ID:** 0000-0002-8074-1647, **CVU CONACYT ID:** 85034

ID 3rd Co-author: *José Marcelino, Gutiérrez-Villalobos* / **ORC ID:** 0000-0001-5947-1489, **CVU CONACYT ID:** 173461

DOI: 10.35429/EJT.2022.12.6.10.15 Received July 20, 2022; Accepted December 30, 2022

Abstract

In this work, a completely automated fiber optic coiling machine for any fiber diameter is presented. This prototype is capable of measuring the length of the fiber while it is coiled, allowing not only to coil large fibers but also to take control of diverse parameters, such as operation speed, and fiber-to-fiber separation. Our own mathematical model was implanted to the brain of the prototype that is based on a pair of stepper motors coupled to spinning rods that control the coiling process. The operation control (brain) is performed by an Arduino microcontroller with its corresponding free software for programming. The mechanical and electrical components selection makes it a low-cost prototype whose functions can be customized depending on the properties of optical fibers through different coiling conditions. Furthermore, we believe it has a good future regarding commercial projection as our approach was conceived independently from any other already registered and/or patented highlighting once again the low cost that would have as a manufactured commercial machine.

Optical fiber coiling, Prototype, Programming Arduino

Resumen

En este trabajo se presenta una máquina enrolladora de fibra óptica completamente automatizada para cualquier diámetro de fibra. Este prototipo es capaz de medir la longitud de la fibra mientras es enrollada, lo que permite no solo enrollar fibras largas sino también controlar diversos parámetros, como la velocidad de operación y la separación fibra a fibra. Nuestro propio modelo matemático se implantó en el cerebro del prototipo que se basa en un par de motores paso a paso acoplados a varillas giratorias que controlan el proceso de bobinado. El control de funcionamiento (cerebro) lo realiza un microcontrolador Arduino con su correspondiente software libre para la programación. La selección de componentes mecánicos y eléctricos lo convierte en un prototipo de bajo costo cuyas funciones se pueden personalizar dependiendo de las propiedades de las fibras ópticas a través de diferentes condiciones de bobinado. Además, creemos que tiene un buen futuro en cuanto a proyección comercial ya que nuestro enfoque fue concebido independientemente de cualquier otro ya registrado y/o patentado destacando una vez más el bajo costo que tendría como una maquina comercial ya terminada.

Enrolladora de fibra óptica, Prototipo, Programación con Arduinos

Citation: RAMÍREZ-HERNÁNDEZ, Miguel Ángel, MEJÍA-BELTRÁN, Efraín, TALAVERA VELAZQUEZ, Dimas and GUTIÉRREZ-VILLALOBOS, José Marcelino. Fiber optic coiling system prototype. ECORFAN Journal-Taiwan. 2022. 6-12:10-15.

* Correspondence to Author (E-mail: emejiab@cio.mx)
† Researcher contributing as first author.

Introduction

A fiber optic coiling system is a machine capable of properly placing, in terms of position and alignment, large specific lengths of optical fiber on a spool. Some commercial instruments that fulfill this function can also calculate the length of the coiled fiber. The difficulty of this process relies in precisely knowing the involved variables in order to estimate the fiber length. These variables include fiber diameter, spool diameter and spool width. In addition, for long fiber lengths the calculations become complicated due to the "spool diameter variations" that result when layers of coiled fiber are completed. In order to accomplish this, it is necessary to have a highly functional mechanical system that places one fiber next to the previous one in each revolution; hence, it is possible to obtain homogeneous layers of optical fiber along the entire width of the spool. As a consequence, the lengths of the corresponding coils of the subsequent layers become precisely known as the compensated spool diameter relies on the number of completed layers.

As a reference, there is a commercial fiber-optic or fine-wire spooler capable of measuring lengths, the Showmark´s DigiSpooler II model (Showmark, 2020). This system offers controlled coiling with adjustable separation between fibers from 10 μm to 100 μm with 1 μm resolution; an adjustable winding speed of approximately 0 rpm -100 rpm, bidirectional winding, fiber break detection, etc. It has a market value of around $40,000 USD to $70,000 USD. On the other hand, a patent search was carried out in the Mexico and the United States databases, searching for systems with similar functions to the prototype presented in this work. In Mexico there are no records of such systems whereas in the US we found two patents, one of them adds on a plastic coating to the fiber and then coils it on the spool (Okada, 2020); the other one is used in telecommunications and spools fiber optic cables of much larger diameters (Kowalczyk et al., 2020). This search for approaches similar to ours was carried out after we completed our work, as our system departed from a particular necessity that we usually have during our regular laboratory work; hence, we minimized possibilities concerning plagiarism from patented approaches.

The description of our work begins by detailing the general structure of our prototype that includes the mechanical parts as well as the programmed and controlled movements. It also describes our mathematical model that was written in the program and allows to estimate the coiled fiber after each spool revolution; it includes experimental results and discussions of the associated errors. Finally, the advantages and future adequations to the prototype are discussed and we conclude with the corresponding section. It is important to highlight that this work represents an improved version, with important functions added, of the previous one that was presented at the *4to Congreso Nacional de Investigación Interdisciplinaria* (Ramírez et al., 2020).

Prototype Structure

On the upper part of the scheme of Figure 1, the main mechanical components are depicted and consist on the rotating spool that receives the fiber (empty spool) which is supported and rotated by Motor 2; the motor is mounted on a sliding platform whose longitudinal movement is produced by a threaded rod that pushes or pulls the platform by means of two parallel rods; at the same time, Motor 1 provides the rotation to the threaded rod that provides the displacement of the empty (fiber receiving) spool; in other words, the Motor 2 provides the rotation of the receiving spool whereas Motor 1 provides the displacement that allows to coil one fiber next to the other. The fiber to be coiled comes from a second spool that is mounted on a slight-friction bearing system; the fiber becomes aligned by means of a pulley that freely rotates on a soft fixture, acting as a strain relief and minimizing in this way the possibility of breaking the fiber. In order to add more fiber alignment, the distance between the strain relief and the feeding spool has to be as long as possible; usually one meter or more is enough. The components were chosen from commercial consumables whose regular use is intended for the 3D-printing industry. Given that the optical fibers are usually very flexible and light in weight, all the system tends to also be very light in weight and, as a consequence, it uses low torque stepping motors and consequently low powers in all the components; i.e., control has preference over power.

ISSN 2524-2121

There is a great variety regarding types of motors used in mechanical systems; however, stepper motors are widely used in systems that require high precision such as ours; based on this, the bipolar stepper motors that we used were the 17HS440-Model (Bello & Luna, 2004) with 200 steps by revolution and 1.8 degrees per step; these resulted very adequate during our tests.

In order to properly control the polarity reversal in both electrical coils of each motor, it is necessary to use an H-bridge per coil since the they demand more current than the maximum that the microcontroller can provide. There are different integrated circuits that include different amounts of H-bridges inside. In our case, a pair of L293b integrated circuits was used, since each one contains 2 H-bridges (Bello & Luna, 2004).

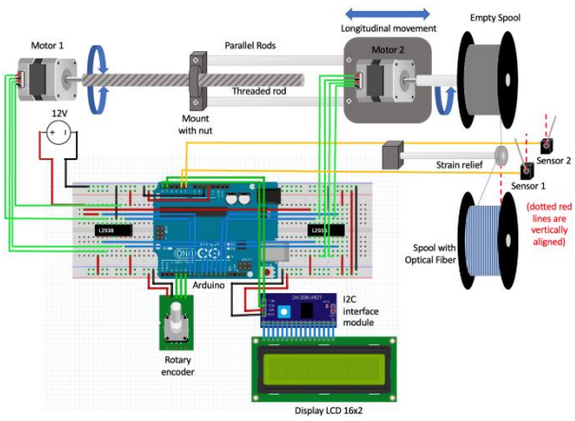

Figure 1 General scheme of the coiling prototype

For controlling the motors through the H-bridges as well as for the general operation of the fiber coiling, we used an Arduino-based programming microcontroller that has an open-source platform that covers our necessities. This is used in multiple electronics projects due to its low cost, ease of use as it is programmed by a C++ simplified version. The model that we used was the ATmega328, which is capable of being programmed and erased/re-programmed with instructions through its free access software. In addition to its simplicity and easy interfacing, it offers the advantage of having multiple independent sensors and other input devices for different purposes (Badamasi, 2014).

In regard to the improvements realized to our previous reported system (Ramírez *et. al*., 2020), we added a pair of limit switches (see Fig. 2) that operate as complete layer indicators; these allow a more automated operation that allows counting layers and reverse longitudinal displacement to start coiling the next layer, and so no. This function was realized manually in the previous version, implying a more human assistance at the end of each layer. Before these sensors were adapted, the operator had to a push bottom at the end of each layer.

The visual interface between the coiling system and the user is a 16x2 LCD display that exhibits a programmed menu as part of the interface for controlling in two operational modes: a) coiling a piece of fiber to determine its length or b) coiling a specific length of fiber. An I2C serial interface board module was used to simplify the programming process as well as the connections.

Once a fiber layer has been completed, the directional change is provided by Sensor 1 or Sensor 2. These are activated by the walls of the receiving spool and command the microcontroller to reverse the rotation of Motor 1 and hence to activate the opposite longitudinal displacement. In this way, with the appropriate number of steps, it is possible to place one fiber next to the other after each turn during the coiling process. On the other hand, while transferring the fiber from the feeding spool to the receiving one, a pulley is used to always feed the fiber in the same place and orientation regardless of the feeding parameters. Additionally, the pulley has a second function as it serves as a strain relief; i.e., the fiber is always tense but not sufficient as to be broken (Ramírez, 2020).

Mathematical model

The method to obtain an equation to calculate any total coiled fiber length starts from an analysis for the simplest case, up to the most complex in which all the variables involved are considered.

In order to know the fiber length in a single revolution on the spool, the expression for the perimeter of a circle $l = \pi d_s$ is used, where l is the length and d_s the spool diameter. This expression can be generalized for any revolution number N obtaining a fiber length L:

ISSN 2524-2121

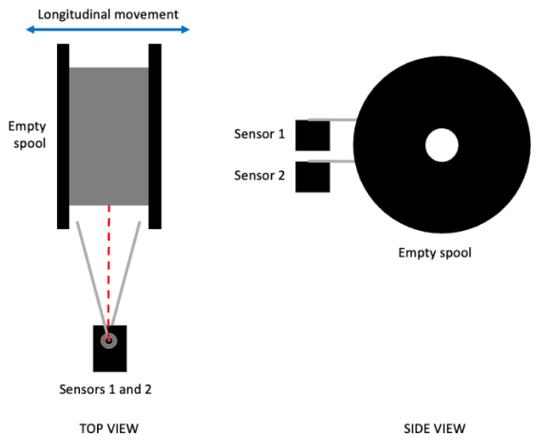

Figure 2 Top and side view of the limit switch sensors

$$L = N\pi d_s \quad (1)$$

However, this expression is only valid within a single layer of coiled fiber. For any subsequent layers, corrections have to be made as follows. As the diameter to perform the calculations will not be the spool diameter but, it will also include twice the diameter of the fiber d_f. Thus, depending on the number of complete layers n, the diameter will increase according to the relation:

$$d_n = d_s + 2nd_f \quad (2)$$

On the other hand, considering a proper tight fiber-to-fiber placement at each revolution on the spool, for each layer of fibers the number of revolutions N can also be represented as the number of fiber diameters that fit in the spool width w_s:

$$N = \frac{w_s}{d_f} \quad (3)$$

Substituting (3) in (1) and considering the diameter increase for each layer of (2), a layer-by-layer analysis can be performed in the form:

$$L_1 = \frac{w_s}{d_f}\pi d_s, \quad 1st\ layer \quad (4)$$

$$L_2 = \frac{w_s}{d_f}\pi[d_s + 2d_f], \quad 2nd\ layer \quad (5)$$

$$L_3 = \frac{w_s}{d_f}\pi[d_s + 2(2d_f)], \quad 3rd\ layer \quad (6)$$

$$L_n = \frac{w_s}{d_f}\pi[d_s + 2(n-1)d_f]. \quad layer\ n \quad (7)$$

Where L_1, L_2 and L_3 are the lengths for the first, second and third complete fiber layers respectively, up to a layer n with length L_n. In this way, to obtain the length of complete layers, L_c for a layer's number n, all the calculated lengths $L_c = L_1 + L_2 + L_3 + \cdots + L_n$must be added, obtaining:

$$L_c = \frac{w_s}{d_f}\pi \sum_{i=1}^{n}[d_s + 2(i-1)d_f] \quad (8)$$

Equation (8) allows us to calculate the fiber length considering only layers filled with fiber. However, in the case of requiring an arbitrary length to be coiled, the length will correspond to a number of complete layers, plus a remaining length L_r as:

$$L_r = N\pi(d_s + 2nd_f) \quad (9)$$

Then, the total fiber length L_T is:

$$L_T = L_c + L_r \quad (10)$$

Experimental Results

Once defined the physical parameters of the receiving spool and the optical fiber diameter, the total revolutions number N_T is obtained by numerically solving (10) with N as unknown, by substituting (8) and (9). Such formulae were introduced in the program in order to obtain the revolutions. Although several tests were realized for calibrating the system, in an example we programmed the prototype for coiling 1km of optical fiber, the system calculated the revolutions (2897.73) and took approximately 2 hours and 10 minutes. For coiling hundreds of meters that are common on experiments with optical fiber in laboratories it does not represent a problem; however, sometimes it is necessary to coil several km and in such a case, the amount of time becomes important. In this sense, further improvements will be necessary to speed up the system.

Associated error

Considering two magnitudes x and y that are obtained through a direct measurement and with associated uncertainty Δx and Δy, respectively; if you want to calculate the uncertainty of an indirect measurement z that is given by $z = x + y$ or $z = x - y$, that is, the sum or subtraction of these measurements, then the uncertainty associated with this variable is the sum of the uncertainties associated with x and y, namely:

ISSN 2524-2121

$$\Delta z = \Delta x + \Delta y \quad (11)$$

On the other hand, if you want to calculate the uncertainty of an indirect measurement w, which can be calculated using the product $w = x \cdot y$, the uncertainty associated with w is given by:

$$\Delta w = |y|\Delta x + |x|\Delta y \quad (12)$$

From (11), the uncertainty or associated error with the coiled length given by (10) can be obtained, then:

$$\Delta L_T = \Delta L_c + \Delta L_r \quad (13)$$

To calculate the fiber length L_c, in (8), the ratio w_s/d_f corresponds to the number of fibers that fit within the spool width used to fill it completely. However, there is an error associated with the limit switch sensors pressing changing the direction of longitudinal movement when completing a full layer of fiber on the spool, this error causes the number of fibers inside the spool not to exactly correspond to the mentioned ratio. Therefore, the ratio w_s/d_f must be substituted as an independent variable c. One way to measure this variable is to perform a statistical analysis for a sample of at least 30 measurements of the number of fibers of a certain diameter (d_f) within a spool of width w_s, in order to obtain the final value associated with the average ($\bar{c}$) of the measurements made, as well as its uncertainty associated with the standard deviation (σ_c) in the form $c \pm \Delta c = \bar{c} \pm 1.96\sigma_c$, to obtain a 95% reliability (Blaine). Thus, by (12), the associated error ΔL_c is:

$$\Delta L_c = c\pi \sum_{i=1}^{n} [\Delta d_s + 2(i-1)\Delta d_f] +$$

$$+\Delta c\pi \textstyle\sum_{i=1}^{n} [d_s + 2(i-1)d_f] \quad (14)$$

On the other hand, the associated error ΔL_r is:

$$\Delta L_r = N\pi\left(\Delta d_s + 2nd_f\right) \quad (15)$$

Finally obtaining:

$$\Delta L_c = c\pi \sum_{i=1}^{n} [\Delta d_s + 2(i-1)\Delta d_f] +$$
$$\Delta c\pi \textstyle\sum_{i=1}^{n} \left[d_s + 2(i-1)d_f\right] + N\pi\left(\Delta d_s + 2nd_f\right) \quad (16)$$

From (16), the statistical analysis for c and considering the resolution of the measuring instrument with which the spool diameter and the fiber diameter were measured as uncertainty associated with d_s and d_f respectively, for 1km of fiber, the associated error is 2.94% (29.4 m).

Advantages

Among the main advantages offered by this device are: its low total cost (~$3500 MXN, compared to commercial devices, around $40,000 USD to $70,000 USD), its compact design compared to the large devices that are found in the market, the multifunctional operation due to access to the programming of the prototype microcontroller, and its performance versatility, due to its ability to coil different fiber diameters and specific lengths, compared to the limited operation of patent-registered devices. In summary, there is a prototype that, even with multiple improvements to be implemented in the future, offers a functional and reproducible coiling service.

Future improvements

The most important aspect to improve is to minimize error as for larger fiber diameters it is higher and hence represents economic issues; for example, when selling a 1-km of optical fiber, the seller must coil at least 1029.4 m to ensure that the fiber is not shorter than promised. Another aspect would be the coiling speed as for several km fibers the time represents up to more than ten hours which represents several risks such as difficulty for human supervision. Several parameters can be induced to the optical properties of the fiber by coiling with certain patterns; loss, birefringence and scattering among other optical properties may be induced in such way. Also, this device can be implemented for more applications such as electrical conductors or even cable coiling of any type (electrical or optical); although, in general, the latter would require much more powerful motors as well as a more heavy and robust mechanical systems. However, thin electrical wires may be coiled and measured with our system as physical properties are similar to the tiny optical fibers.

ISSN 2524-2121

Conclusions

It was possible to develop a prototype fully automated capable of coiling and measuring large amounts of optical fiber while transferred from one spool to another in a controlled, uniform and homogeneous manner. Due to having control over parameters such as the coiling speed and the separation distance between fibers, it can be programmed to calculate the coiled fiber length. In this way, an adaptable system with adjustable functions is obtained for fiber optics laboratories and industries that require to induce or reduce values of some parameters in coiled optical fibers.

Acknowledgements and funding

This work has been supported by CONACYT [scholarship No. 742457]. We also thank to Álvaro A. Guerra Him for technical support during the system preliminary tests.

References

Showmark. (2020). *DigiSpooler I & II*. https://www.showmarkcorp.com/product/digispooler/

Okada, K. (2020). *Bare optical fiber coating device and bare optical fiber coating method* (Patent Application No. 20160083293). https://www.patentsencyclopedia.com/app/20160083293

Kowalczyk, S., Smith, T., Kaml, J., LeBlanc, T., & Beck, R.. *Fiber optic enclosure with external cable spool* (Patent Application No. 20080292261). https://www.patentsencyclopedia.com/app/20080292261

Ramírez, M. (2020). *Desarrollo, diseño e implementación de un prototipo estrechador de micro-fibra óptica (Master's thesis)* [Centro de Investigaciones en Óptica]. https://bibliotecas.cio.mx/tesis/17887.pdf

Bello, I. I. H., & Luna, C. O. (2004). *Control difuso y construccion de un mecanismo capaz de golpear con distintos efectos una bola de billar (Bachelor's thesis)* [Universidad de las Américas Puebla.]. http://catarina.udlap.mx/u_dl_a/tales/documentos/lep/hernandez_b_ii/

Badamasi, Y. A. (2014, December 23). The working principle of an Arduino. *Proceedings of the 11th International Conference on Electronics, Computer and Computation, ICECCO 2014*. https://doi.org/10.1109/ICECCO.2014.6997578

Ramírez, M., Mejía, E., & Juárez, M. (2020). Enrolladora de fibra de bajo costo hecha en casa. In Memories of *4to Congreso Nacional de Investigación Interdisciplinaria. Instituto Politécnico Nacional*. Publication pending.

Blaine. *Understanding Precision Statements for Standard Reference Materials*. http://www.tainstruments.com/pdf/literature/TN061%20Understanding%20Precision%20Statements%20for%20Standard%20Reference%20Materials.pdf.

ISSN 2524-2121

Article **ECORFAN Journal-Taiwan**
December 2022, Vol.6 No.12 16-23

Analysis of bathymetric surfaces for the determination of sediments in the inner basin of the port of Salina Cruz, Oaxaca

Análisis de superficies batimétricas para la determinación de sedimentos en la dársena interior del puerto de Salina Cruz, Oaxaca

TREJOLIEVANO-DE LA ROSA, Carlo Saddam†*, AGUILAR-RAMIREZ, Ana María, DOMÍNGUEZ-GONZÁLEZ, Agustín and MOLINA-NAVARRO, Antonio

Instituto Oceanográfico del Golfo y Mar Caribe.

ID 1st Author: *Carlo Saddam, Trejolievano-de la Rosa* / **ORC ID:** 0000-0002-8614-7091, **CVU CONACYT ID:** 1003850

ID 1st Co-author: *Ana María, Aguilar-Ramírez* / **ORC ID:** 0000-0003-2867-8254, **CVU CONACYT ID:** 811392

ID 2nd Co-author: *Agustín, Domínguez-González* / **ORC ID:** 0000-0002-3199-5771, **CVU CONACYT ID:** 811473

ID 3rd Co-author: *Antonio, Molina-Navarro* / **ORC ID:** 0000-0001-7949-8371, **CVU CONACYT ID:** 811437

DOI: 10.35429/EJT.2022.12.6.16.23 Received July 20, 2022; Accepted December 30, 2022

Abstract

The Bathymetric Surface is original data from a bathymetric survey, or a cloud of points resulting from a subsequent edition keeping the associated metadata, can be processed based on a reticulated structure representing the geometry of the seabed as faithfully as possible, for a area of sea, river, lake or other navigable water, the primary objective of this work is to analyze the bathymetric surfaces derived from hydrographic surveys, to determine how the dragging of sediments has affected the depth in the inner dock of the port of Salina Cruz , Oaxaca. Due to the above, bathymetric data were obtained from the surveys carried out in the years 2010, 2018 and 2021 with the CEEDUCER PRO and R2 Sonic 2024 echosounder, the Hypack and CARIS BASE Editor programs were used for the management and validation of bathymetric data and to obtain the surfaces bathymetric at each time from the surveys and compare the interpolation models that generate the aforementioned surfaces derived from each survey. The results indicate that there are areas with greater sediment deposition where a depth ranging from 10 cm to 1.20 m has been lost according to the last bathymetry carried out in 2021, in order to provide safety conditions for navigation in the area of smaller vessels, tugboats, pilot vessels and vessels in general.

Bathymetric surfaces, Depth, Sedimentation

Resumen

La Superficie Batimétrica son datos originales de un levantamiento batimétrico, o una nube de puntos resultante de una edición posterior manteniendo los metadatos asociados, se pueden procesar en base a una estructura reticulada representando de la forma más fiel posible la geometría del fondo marino, para un área de mar, rio, lago u otra agua navegable, el objetivo primordial del presente trabajo es analizar las superficies batimétricas derivadas de los levantamientos hidrográficos, para determinar cómo ha afectado el arrastre de sedimentos a la profundidad en la dársena interior del puerto de Salina Cruz, Oaxaca. Por lo anterior se obtuvieron datos batimétricos de los levantamientos efectuados en los años 2010, 2018 y 2021 con la ecosonda CEEDUCER PRO y R2 Sonic 2024, se utilizaron los programas Hypack y CARIS BASE Editor para la gestión y validación de datos batimétricos y obtener las superficies batimétricas en cada época a partir de los levantamientos y comparar los modelos de interpolación que generan citadas superficies derivadas de cada levantamiento. Los resultados indican que existen zonas con mayor deposición de sedimentos donde se ha perdido una profundidad que va desde los 10 cm hasta el 1.20 m de acuerdo a la última batimetría realizada en el año 2021, a fin de proveer condiciones de seguridad para la navegación en el área de las embarcaciones menores, remolcadores, buques piloto y buques en general.

Superficies batimétricas, profundidad, sedimentación

Citation: TREJOLIEVANO-DE LA ROSA, Carlo Saddam, AGUILAR-RAMIREZ, Ana María, DOMÍNGUEZ-GONZÁLEZ, Agustín and MOLINA-NAVARRO, Antonio. Analysis of bathymetric surfaces for the determination of sediments in the inner basin of the port of Salina Cruz, Oaxaca. ECORFAN Journal-Taiwan. 2022. 6-12:16-23.

* Correspondence to Author (E-mail: carlosaddam181090@gmail.com)
† Researcher contributing as first author.

Introduction

Bathymetric surfaces consist of a set of grid values arranged to form a coverage representing a bathymetric depth model for an area of sea, river, lake or other navigable water. The data set includes both the estimated depth values and the uncertainty estimates associated with the depth values. That is, the dataset can carry both measured depth information that can be used for scientific purposes and corrected depth information that can be used for navigation (KHOA Korea Hydrographic and Oceanographic Agency, 2019).

Basile (2018) in his book "Sediment transport and morphodynamics of alluvial rivers" defines this concept as the granular solid material found in the bed of a river, basin, lake or coast which has been transported and deposited by the action of marine currents or other transport methods along its morphological evolution.

Silt is a deposit of sediment, which is carried by water and accumulated in riverbeds, dams, underground reservoirs, wetlands, lagoons, estuaries, navigation channels, harbours, etc., is called silt. The cause of siltation is a decrease in the velocity of the current and a corresponding decrease in the amount and size of solid material that can be carried in suspension. Thus, siltation is the phenomenon in which sediment accumulates and results in the transformation of the environment (Carbajal, 2014).

The equipment used for the hydrographic surveys included the CEEDUCER PRO single beam echo sounders and the R2 SONIC 2024 Multibeam Multibeam. The data acquired by means of this equipment provide a bathymetric surface with a resolution of even less than one metre, which results in a high-resolution configuration of the seabed.

The single-beam echo sounder is a type of electronic instrument that has a transducer that generates a single acoustic pulse (all the acoustic energy transmitted is confined to a single beam that has a cone-like shape) that reaches the seafloor, so it is not possible to obtain 100% coverage of the bottom, and it is necessary to make lines at a certain distance without being able to know what is between them (sectors without information) (Ballestero, 2010).

The use of multibeam echo sounders for bathymetry has become the most developed and accurate technology available today. This system, which complies with International Hydrographic Organisation (IHO) standards, provides accurate and complete knowledge of the depth and morphology of the seabed. This Multibeam system consists of a set of sounders that emit several narrow beams of sound in different directions, arranged in the shape of a fan that sweeps transversely in the direction in which the vessel is moving (Basile, 2018).

The port of Salina Cruz, Oaxaca, has a great relevance in the Mexican Pacific, as it is characterised by handling cargo traffic from the South (S) and Southeast (SE) region of the Mexican Republic, which includes the states of Oaxaca, Chiapas, Veracruz, Campeche, Tabasco, Puebla, among others. This port comprises the outer harbour, whose access is formed by two breakwaters and the dock, which communicates with the outer harbour through the channel called entrepuente (Administración Portuaria Integral, 2021).

Figure 1 shows the port's terminals and facilities, showing the inner manoeuvring dock with an approximate diameter of 300 m, where ship construction, repair and maintenance activities are carried out, as well as shipments of gas and refined products. In addition, work related to the fishing industry is carried out and the city's municipal waters are discharged.

Figure 1 Port terminals and facilities
Source: Own elaboration

ISSN 2524-2121

Currently, the port of Salina Cruz, Oaxaca has a draught of 12 metres (m) in the navigation channel and 10 m in the inner dock, with 20.3 hectares (ha) for navigation. To date, the port has 14 berths for ships of greater draught, distributed in two terminals: a terminal for public use that handles bulk mineral, agricultural, containers and general cargo; and a terminal for private use, operated by Petróleos Mexicanos (PEMEX) for the storage and transport of petroleum fuels (Secretaria de Comunicaciones y Transportes, 2016).

This analysis focuses on the inner dock, shown in Figure 2, which is an area where vessels of more than 100 m. in length, up to smaller vessels that carry out the transfer of "pilot/practical" personnel that support the arrival of cargo ships, manoeuvre in and out of the port.

The Ministry of the Navy (SEMAR) has the ASTIMAR-20 where all ships entering for maintenance and repairs do so from the inner dock. Likewise, all the tugboats that provide support and push services to the larger vessels that arrive at the PEMEX terminal to load petroleum products are located in this basin.

Figure 2 Inner dock of the port of Salina Cruz, Oaxaca
Source: El Imparcial de Oaxaca, 2018

Methodology

This research was carried out by means of bathymetric data, acquired according to the established bottom coverage standards (IHO, 2008) in the inner harbour basin of the port of Salina Cruz during the years 2010, 2018 and 2021, with the R2 Sonic 2024 and CEEDUCER PRO multibeam echo sounders described in Table 1, which are presented in Figure 3. The R2Sonic 2024 and CEEDUCER PRO echo sounders have the following characteristics:

Characteristics Type	Echo sounders	
	R2 SONIC 2024	CEEDUCER PRO
Frequency	Multibeam	Monohaz
Beamwidth across the scan	400 kHz/ 200 kHz	200 kHz / 30 khz
Number of beams	0.5 ° @400 kHz /1.0° @200 kHz	No scanning beam
Scanning angle	256	1 pulse per second
Pulse length	10° to 160° (user selectable)	Does not count
Pulse type	15µ Sec- 1000 µ Sec	Not specified
Depth range	Continuous waveform (CW)	1 pulse per second
Operating temperature	100 metres (3000 metres optional)	0.3- 99.9 m 0.75- 99.9 m
Storage temperature	-10°C to 40°C	0°C to 50°C
Characteristics	-30°C tp 55°C	Not specified

Table 1 System Specification of the R2 Sonic 2024 and CEEDUCER PRO echo sounders
Source: Operation manual R2 Sonic, 2024 and CEEDUCER PRO

Figure 3 shows the R2Sonic 2021 and CEEDUCER PRO echosounder and its modular interface.

Figure 3 Echosounder R2Sonic 2021 and CEEDUCER PRO and modular interface
Source: R2 Sonic 2024 and CEEDUCER PRO (2019) operation manual

Firstly, the Hypack 2021 programme in its version 1.21 was used to generate bathymetric surfaces for each epoch, and then, using one of the software tools called "TIN model" (Triangle Irregular Network), the data was processed to determine the sediment volume.

ISSN 2524-2121

The "TIN model" generates a type of vector-based digital geographic data that is constructed by triangulating a set of vertices (points). The vertices are connected with a series of edges to form a network of triangles. In other words, they connect three probes to make a triangular "face" (Figure 4). The faces can then be used to represent a bathymetric surface detailing volumes created from these triangles.

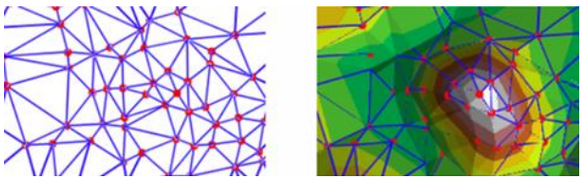

Figure 4 Creation of TIN models
Source: Hypack (2021)

The result after the creation of the TIN model (Figure 5), is the comparison between two accurately overlapping bathymetric surfaces, generating a report which, from the network of triangles, determines the volume of sedimentation added and removed, in this case in the interior of the manoeuvring basin of the port of Salina Cruz, Oaxaca.

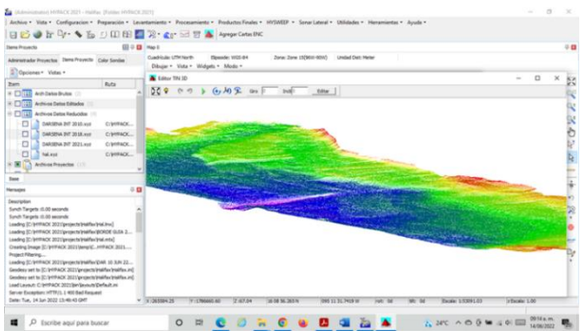

Figure 5 TIN model, from the bathymetric surfaces
Source: Hypack (2021)

On the other hand, with the CARIS Base Editor program, the bathymetric surfaces were generated from the same sounding data with which the TIN models were made in Hypack, in order to maintain the same information used and to serve as a point of comparison.

The bathymetric surfaces were generated through "XYZ" files (Figure 6), which contain the information on coordinates and depths, using the WGS84 reference datum.

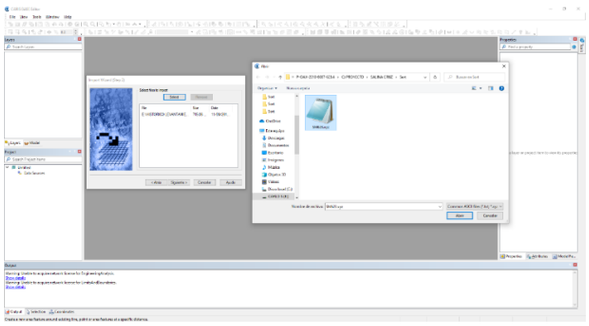

Figure 6 Import of bathymetric data from the XYZ file.
Source: CARIS Base Editor

The subsequent result was a bathymetric surface in two and three dimensions (Figure 7) for each year (2010, 2018 and 2021), where details of the seabed can be observed, distributed uniformly and by colour, in order to obtain a clear idea of the configuration of the area in question.

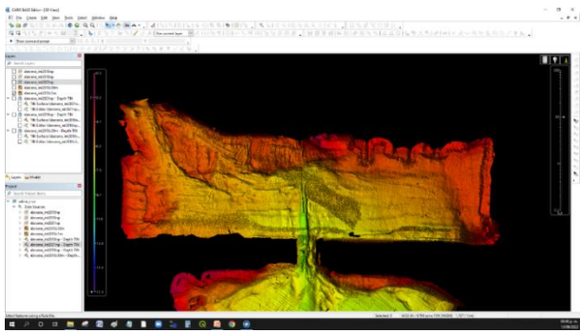

Figure 7 Bathymetric surface of the year 2010.
Source: CARIS Base Editor

Once the bathymetric surfaces for each year have been generated, the CARIS Base Editor program has a tool called "coverage difference" which, by interpolating two surfaces, generates a third one, which is the result of the difference between the two.

Results

The TIN models, described in the methodology of this article, generated from the data processed in Hypack, were merged, using the tool "TIN models", generating a report for the comparison of the bathymetric surfaces 2010 - 2018 (Figure 8) and 2018 - 2021 (Figure 9).

ISSN 2524-2121

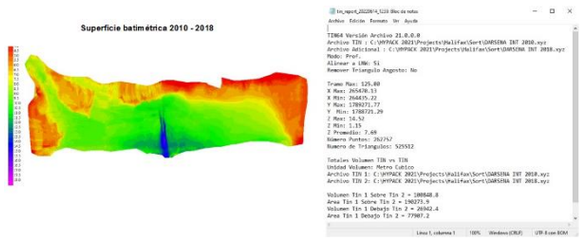

Figure 8 2010 - 2018 bathymetric surface and sediment report
Source: Hypack, (2021)

On the left of Figure 8 is the two-dimensional bathymetric surface generated from the interpolation of the 2010 and 2018 bathymetric surfaces, showing the soundings obtained during the 2010 and 2018 surveys, overlaid on top of one another. The depth scale shows the shallowest soundings from 4 m to the deepest areas at 18 m, which are located in the centre of the basin (coloured in blue), which belongs to the access channel and the passage from the interchange to the outer basin.

On the right side of Figure 8 is the report that generated the comparison of the bathymetric surfaces indicating that 525,512 triangles were generated from the existing sounding points, volume TIN 1 over TIN 2 indicates the amount of 100, 848.8 m3 that represents the matter that has been removed, while volume TIN 1 under TIN 2 indicates the amount of 26, 924.4 m3 that represents the matter that has been added, i.e. the sediments deposited during that period.

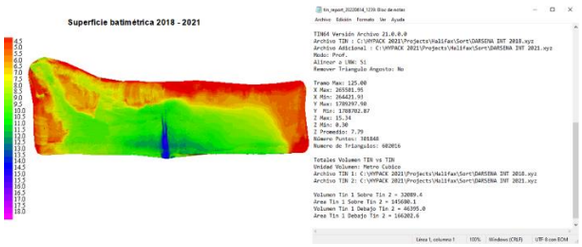

Figure 9 Bathymetric surface 2018 - 2021 and sediment report
Source: Hypack, (2021)

On the left hand side of Figure 9, the bathymetric surface derived from the 2018 - 2021 comparative, it shows a greater red colouring, which represents shallow depths, most noticeably in the area adjacent to the docks and the entrance to ASTIMAR-20.

This trend is reflected in the report generated by Hypack, which we can see on the right of Figure 9, which tells us that 602,016 triangles were generated from the existing sounding points, the volume TIN 1 above TIN 2 indicates the amount of 32,089.4 m3 which represents the material that has been removed, while the volume TIN 1 below TIN 2 indicates the amount of 46,395 m3, which corresponds to the material that has been added.

As part of the work carried out in the CARIS Base Editor program, bathymetric surfaces were generated for the years 2010 and 2018 (Figure 10).

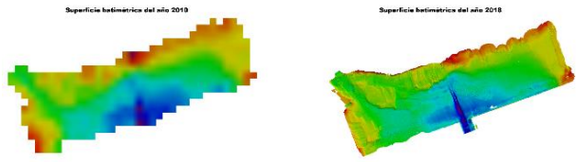

Figure 10 Bathymetric surfaces for the years 2010 and 2018
Source: CARIS Base Editor

Once the bathymetric surfaces for the years 2010 and 2018 were obtained, by means of the methodology described above, a third bathymetric surface was generated, which corresponds to the difference in depths found between each one, as shown in Figure 11.

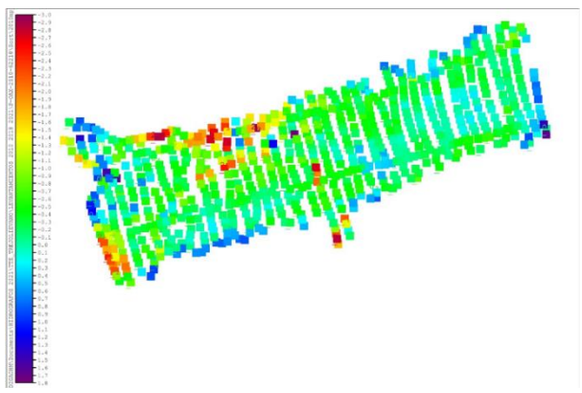

Figure 11 Difference in depths between the years 2010 and 2018
Source: CARIS Base Editor

The blue colour represents an average of 0.5 metres of depth that has been lost over the years, which is noticeable in clustered areas, which supports that the amount of 26, 924.4 m3 reported by the Hypack programme as deposited matter, is almost uniformly dispersed along the basin, showing areas with a higher concentration of sediment.

The bathymetric surfaces for the years 2018 and 2021 (Figure 12), also generated in CARIS Base Editor, are presented below. These surfaces have a higher resolution as both were obtained from data acquired with the R2 Sonic 2024 echosounder.

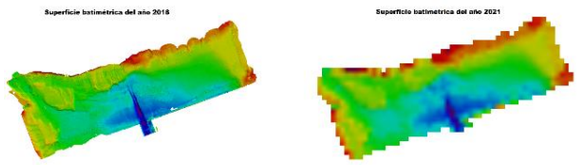

Figure 12 Bathymetric surfaces for the years 2018 and 2021
Source: CARIS Base Editor

In the same way, the bathymetric surfaces of the years 2018 and 2021 were interpolated, thus generating a third bathymetric surface, which corresponds to the difference in depths between the years 2018 and 2021 shown in Figure 13.

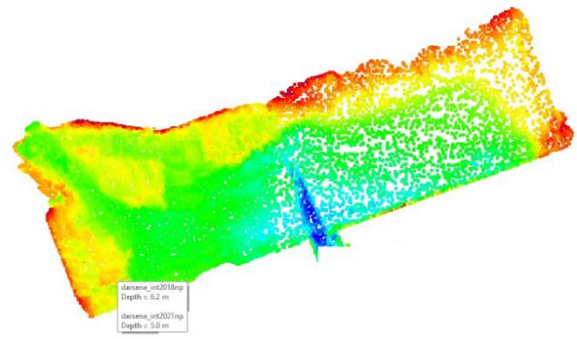

Figure 13 Difference in depths between years 2018 and 2021
Source: CARIS Base Editor

This bathymetric surface shows one of the most representative areas where depth has been lost, as in 2018 there were 6.2 metres, compared to 2021 where soundings of 5.0 metres are recorded, strictly speaking, there are areas where the depth has decreased to 1. 2 meters, corresponding to this surface, according to the report generated by Hypack the amount of 46,395 m3 of matter that has been deposited, observing a tendency of concentration in the vicinity of the docks, and not so in the centre of the dock.

Based on the above, and with the CARIS Base Editor program, a 3-D view (X10 exaggeration) of the seabed (Figure 14) was obtained for the year 2021, in order to observe the configuration of the seabed and to determine the areas most vulnerable to sedimentation.

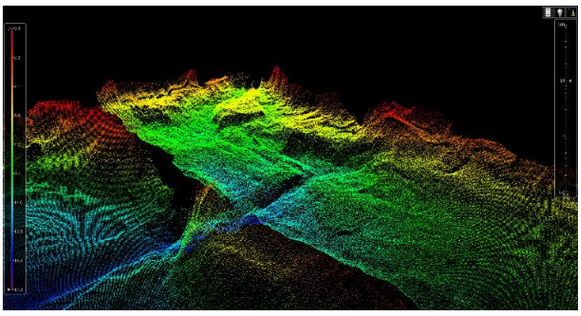

Figure 14 Seabed in the inner harbour in the year 2021
Source: CARIS Base Editor

Areas in yellow and red can be clearly seen, which belong to the vicinity of the dock, where there are submarine mounds, which due to their characteristics are difficult to remove by dredging, being therefore places where, with the passage of time, sedimentation adheres and leads to the loss of depth and therefore a danger to navigation, but especially for ships with drafts greater than 3 metres.

Conclusions

By means of the Hypack and CARIS Base Editor programs, the bathymetric surfaces were analysed, obtaining the volume of sediment (added and removed material) by means of Hypack and TIN models, while by means of the CARIS Base Editor program, the difference in depths was obtained for each model, being represented in two and three dimensions, thus locating the most vulnerable areas, where sedimentation has not been removed and causes a loss of depth.

It was verified that it is possible to determine the volume of sediments, from the analysis of bathymetric surfaces in Hypack, using the CARIS Base Editor program as a method of help and verification, thus determining that the areas where there is a greater loss of depth are those near the docks and the entrance to the Navy Yard No. 20.

ISSN 2524-2121

Recommendations

Dredging should be carried out in the inner dock of the port of Salina Cruz, on a constant and permanent basis, being recommended at least once a year. Likewise, and prior to works of this nature, it is proposed that a soil mechanics study be carried out, aimed at the foundations of the dock, in order to determine the scour generated by the fluid dynamics, so as to be certain that dredging can be carried out in the vicinity of the docks or that modernisation or reinforcement of structures is necessary.

The port of Salina Cruz, Oaxaca, is no stranger to the problem of siltation and sediment transport, according to Carmona (2006) in the study he carried out in the area, entitled "Application of civil engineering to the problem of beach erosion in the region of La Ventosa Bay in Salina Cruz, Oaxaca", in which he writes how the coastal area near the port has suffered a decrease in depth due to the breaking of waves near the beach line and breakwaters, which causes turbulence in the flow and consequently the suspension and dragging of granular material.

Derived from the above, the inner harbour of the port of Salina Cruz also presents a dragging of sediments that, due to different causes, such as runoff and turbulence in the flow of currents, generate silt and sedimentation, being the main problem that causes the loss of depth. Another important factor is the estuaries present in the area, which are located between the rivers and the coasts and act as material traps, causing a deficit in the beach area, which is why it was necessary to analyse the bathymetries carried out in the inner dock for the years 2010, 2018 and 2021. The most significant variables for the study were depth and sediments. The Hypack and CARIS BASE Editor programmes were used to process them, in order to achieve the objective of analysing the bathymetric surfaces for the determination of sediments in the inner basin, with the aim of providing greater safety and confidence to the navigators who use the port (Carmona, 2006).

Likewise, the Administración Portuaria Integral (API) in its report "Manifestación de impacto ambiental modalidad regional para la modernización del puerto petrolero y comercial del puerto de Salina Cruz, Oaxaca (2021)" describes the importance of carrying out a dredging project, due to the need to increase the depth in the oil and commercial area to allow the arrival of larger vessels, as the depths of the navigation channel and manoeuvring basin are not adequate.

References

Abel Basile, Pedro. 2018. “Transporte de Sedimentos y Morfodinámica de Ríos Aluviales”.

Administración Portuaria Integral (API) 2021. “Manifestación de impacto ambiental modalidad regional para la modernización del Puerto Petrolero y Comercial Del Puerto De Salina Cruz, Oaxaca”.

Ballestero-Mora, L. y García-Sala, D. 2010. “Estudio Batimétrico con ecosonda multihaz y clasificación de fondos”. Universidad Politécnica de Cataluña.

Carbajal-Evaristo, Sarahi & Hernández, Cristian & Díaz-Gallegos, José & Mata, Dulce & Acosta-Velázquez, Joanna. (2014). Evaluación del impacto del azolvamiento en la Laguna Cerritos como consecuencia de la canalización del río Cintalapa, Chiapas.

Hugo Carmona Gómez. 2016. “Aplicación de la Ingeniería Civil al Problema de Erosión Playera en la Región de la Bahía de la Ventosa en Salina Cruz, Oaxaca”.

Korea Hydrographic and Oceanographic Agency. 2019. http://www.khoa.go.kr

OHI. 2020. “Normas de la OHI para los Levantamientos Hidrográficos publicación S-44”. Mónaco Bureau Hidrográfico Internacional.

Secretaria de Comunicaciones y Transportes. 2016. “Programa maestro de desarrollo portuario del puerto de Salina Cruz 2016-2020”.

Hypack. 2021. Hypack. Manual de referencia https://www.hypack.com/File%20Library/Resource%20Library/Manuals/2021/HYPACK-2021-User-Manual_SP.pdf

ISSN 2524-2121

Ceehydrosystems. 2021. CEEDUCER PRO. *Ficha técnica* http://www.ceehydrosystems.com/Downloads/CEEDUCER%20PRO_web.pdf

R2SONIC. 2022. R2SONIC. *Ficha técnica* https://www.r2sonic.com/products/sonic-2024.

ISSN 2524-2121

Article **ECORFAN Journal-Taiwan**
December 2022, Vol.6 No.12 24-28

Cost-effective automatic winder machine for optical fiber filament

Devanadora automática de bajo costo y precisión para filamento de fibra óptica

GUTIERREZ-VILLALOBOS, José Marcelino†, TALAVERA-VELÁZQUEZ, Dimas, MEJÍA-BELTRÁN, Efraín and RAMÍREZ-HERNÁNDEZ, Miguel Ángel

Universidad de Guanajuato Campus Celaya-Salvatierra, Av. Javier Barrios Sierra 201 Col. Ejido de Santa María del Refugio C.P. 38140 Celaya,-Gto. México.
Universidad Autónoma de Querétaro, Cerro de las Campanas s/n, C.P. 76010, Querétaro, Querétaro, México.

ID 1st Author: *José Marcelino, Gutierrez-Villalobos* / **ORC ID**: 0000-0001-5947-1489, **Research ID Thomson**: S-7666-2018, **CVU CONACYT ID:** 173461

ID 1st Co-author: *Dimas, Talavera-Velazquez* / **ORC ID**: 0000-0002-8074-1647, **CVU CONACYT ID:** 85034

ID 2nd Co-author: *Efrain, Mejia-Beltran* / **ORC ID**: 0000-0001-8960-6604, **CVU CONACYT ID:** 20998

ID 3rd Co-author: *Miguel Ángel, Ramirez-Hernandez* / **ORC ID**: 0000-0002-6093-090X, **CVU CONACYT ID:** 742457

DOI: 10.35429/EJT.2022.12.6.24.28 Received July 20, 2022; Accepted December 30, 2022

Abstract

In the market of equipements to wind optical fiber, there are winding machines, which are usually expensive and the ones that are not expensive, can present an important error at the moment to make large fiber rolls in the order of kilometers, these rolls cab be used for selling, storage or for instrumentation applications (in this case, using the optical fiber as sensor to measure some variables such as structure deformation, etc). That is way is necessary to have an equipment, that allow to wind large stretches of fiber at a low cost and effectivity. A propose of a small error winding is presented in this work, a good alternative is shown in this project by using a low-cost micro controller and semiconductors.

Optical fiber inovation, Instrumentation, automation, Winding machine alternative

Resumen

En el mercado de quipos para devanar fibra óptica, existen maquinas embobinadoras que suelen ser costosas y las que no son costosas pueden presentar un error considerable al momento de hacer rollos de fibra que sean de longitudes grandes en el orden de kilómetros, lo que puede llevar a un desperdicio de material cuando se realizan dichos rollos, ya sea para sus venta, almacenamiento o para aplicaciones de instrumentación (utilizando la fibra como un sensor para medir alguna variable, como deformación de estructuras, etc). Por lo que es necesario contar con un equipo que permite devanar tramos largos de fibra óptica a un bajo costo y con efectividad. Este trabajo, ofrece una propuesta de un sistema que presenta un bajo error a la hora de crear rollos de fibra y resulta una propuesta económica al utilizar un microcontrolador y semiconductores de bajo costo.

Innovación en fibra óptica, Instrumentación, Automatización, Alternativa de bobinado

Citation: GUTIERREZ-VILLALOBOS, José Marcelino, TALAVERA-VELÁZQUEZ, Dimas, MEJÍA-BELTRÁN, Efraín and RAMÍREZ-HERNÁNDEZ, Miguel Ángel. Cost-effective automatic winder machine for optical fiber filament. ECORFAN Journal-Taiwan. 2022. 6-12:24-28.

† Researcher contributing as first author.

Introduction

For optical fiber filament winding, a winding machine is a necessary tool to make work easier. Several wire and optical fiber filament winding machines have become a topic of interest for many aspects such as tension control, wire aligning, system control and control by vision, among others. When the time for copper wire winding is needed, a control torque scheme is suitable depending on the wire gauge, as explained by Deng 2021. For thin wire diameters, tension control is required in order to keep turns identically wound, opposite to thick wires, where torque regulation is a must to ensure winding process continue running despite the stiffness of the wire. On the other hand, for optical fiber filament, high-speed and precision alignment control is mandatory to wind long lengths of filaments. In addition, some other works based their investigations on the economic impact using these systems to increase the amount of filament spool productions as reported Ferrer-Alos and Sanchez 2022.

Several optical fiber filament winding machines have been reported in literature, such as the systems described by Campos 2022, Ming 2011 and Ferrer-ALOS 2022, where fiber stress analysis is taken into consideration into their mathematical model and an error method is presented, respectively.

The importance of reducing the winding error lays on the fact that for long length of optical fiber filament multiply by the error, will lead us to a considerable material waste. In Kanade 2018, that fact is mentioned and a control algorithm is well described and implemented on a micro controller to ensure a proper material distribution.

Other works related to winding optical fiber include digital image processing, tensors methods, where the aligning angle is observed and computed by image recognition, this may lead to an expensive approach, as described by Mosquera 2022 and Kang 2020. Finally, it is important to mention some applications for optical fiber coil, such as sensor for sea floor seismic Monitoring (Chen et all, 2016), optical fiber gyroscope (Korkishko 2011) and

Fiber winding systems

Essentially, Optical fiber winding machines are conformed by a mechanic part to hold the spool and another part to align the filament along the spool, as it can be observed on figure 1.

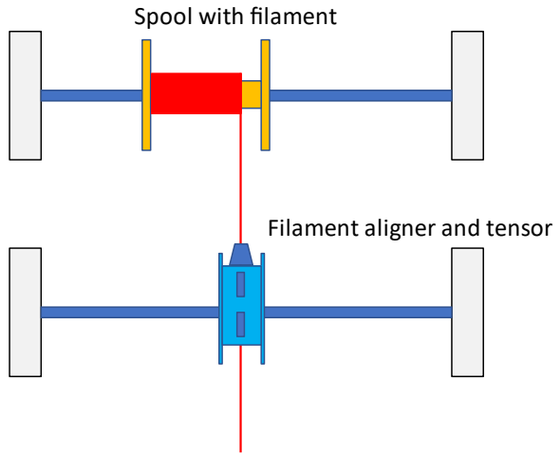

Figure 1 Basic winding machine scheme

The coil wounded upon the spool is formed by the movement of the aligner, which distributes the optical filament on the spool surface, while the tensor is necessary to keep a constant tension on the filament during the aligner displacement. Before this action takes place, system has to ensure the amount of optical fiber filament fits in the spool size, so the number of turns and layers must be calculated in advanced.

Each turn is measured by a motor-shaft-connected incremental encoder, once the number of turns is accomplished on each layer, the aligner starts going backward to make the next layer, and so on.

System operation

In the system functioning, there are some steps to follow. First, the spool inner and outer diameters and optical fiber filament must be set in its place and alighted by the interface using the keys on the keyboard, the alignment is control by the Time-Of-Flight (ToF) sensor and the aligning car. That car is moved by a stepper motor. Second, spool and filament must be introduced on the display interface, number of turns and layers must be calculated and compared to see if they fit in the spool, the result is then display so user can know if the spool is suitable for the amount of optical fiber filament and the spool.

ISSN 2524-2121

This sequence is shown in the block diagram of the figure 2. If the optical fiber filament does not fit in the spool, the system interface sends an alert message to indicate to chance the spool size or the amount of filament to wind, after new parameters need to be introduced; finally, the system again has to calculate if the design is going to fit.

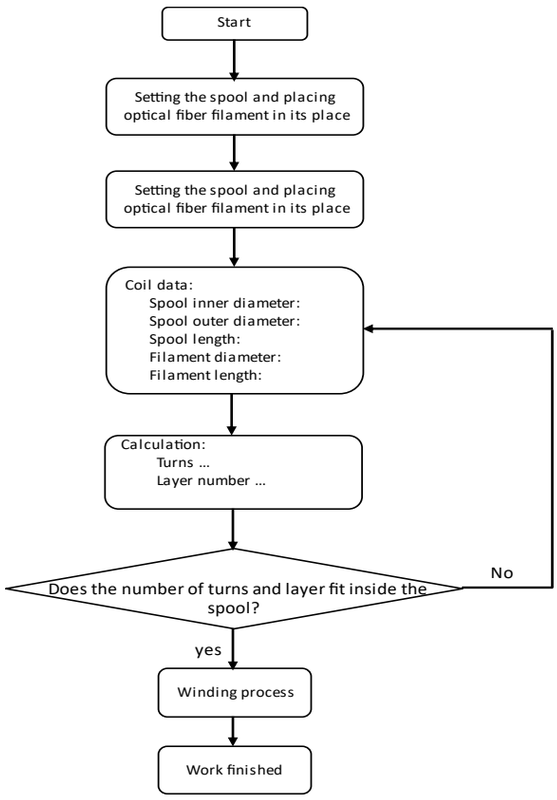

Figure 2 Block diagram for machine sequence operation

Base on this algorithm, the design is easier to understand and the procedure is friendly to follow and the user can performance a design.

Error estimation

In order to estimate the number of turns, layers and error, the following algorithm is implemented in the system board:

```
d1=0;% spool inner diameter (mm)
d2=0;% spool outer diameter (mm)
d3=0;% optical fiber filament diameter (mm)

L=0;% spool inner length (mm)
Lf1=0;% optical fiber filament length (m)
Lf2=0;% aux optical fiber filament length (m)

Nturns=0;% number of turns (#)
Rad1=0;% spool inner radio (mm)
% Proceso
d1=input('spool inner diameter (mm)=');
d2=input('spool outer diameter (mm)=');
d3=input(‘optical fiber filament diameter (mm)=');

L=input(‘spool inner length (mm)=');
Lf1=input('longitud de la fibra (m)=');
Lf2=Lf1*1000; % contertions from m to mm
Rad1=d1/2;
Nturns =fix((L/d3));% number of turns (#)

i=0;
Cont1=0;
Lacum=0;
Cond=1;
Turn=0;
while Cond==1
  Lacum=Lacum+(2*pi*(Rad1+(d3*i)));
  Cont1=Cont1+1;
  Turn=Turn+1;
  if Cont1== Nturns
     i=i+1;
     Cont1=0;
  end

  if Lacum>=Lf2
     Cond=0;
  else
     Cond=1;
  end
end
disp(Spool Thickness mm');
Res=d2-d1
disp('Layer Hight mm');
Alt=fix(d3*i)
if Res<Alt
   disp('Design does not fit');
else
   disp('Design fits')
end
disp('optical fiber filament length en mm');
disp(Lf2)
disp(‘acumulated optical fiber filament length en mm');
disp(Lacum);
disp('Number of layers');
disp(i);
disp('Number of turns per layer');
disp(Nturns);
disp(‘Total number of turns);
disp(Turn);

error=((Lacum-Lf2)/Lf2)*100;

disp(‘The % of error is=')
disp(error)
```

ISSN 2524-2121

System proposed

The winding system is conformed by an ATmega2560 microcontroller embedded in a fast-development board with pin connectors, which simplifies its implementation. A ToF sensor (VL53L4CD) with a resolution of millimeters to detect where the spool is located on the horizontal axe, then to be able to set its point of start (home) for the aligner car in order to star winding the filament. To move the aligning car, a stepper motor is activated by a set of pulses sent by the system board, as mentioned before, the stepper is a NEMA 17HS2408 bipolar model (4.8 Volts, 0.6 Amps and 1.2 Kg/cm). A LPD3806-400BM-G5-24C AVP incremental rotary encoder of 400 PPR and 5V-24V. A DC-24V 24W motor with gear box CW/CCW (24V 150rpm). Also, a 16X2 LCD module for user interface, a EasyDriver - Stepper Motor Driver A3967 Microstepping board, a 4x4 hard Atmel Pic keyboard, and finally, 5V 12V 24V 15A Dual h-bridge DC module (CZB6721960). Each part and stages of the system is shown on figure 3, with their interconnection.

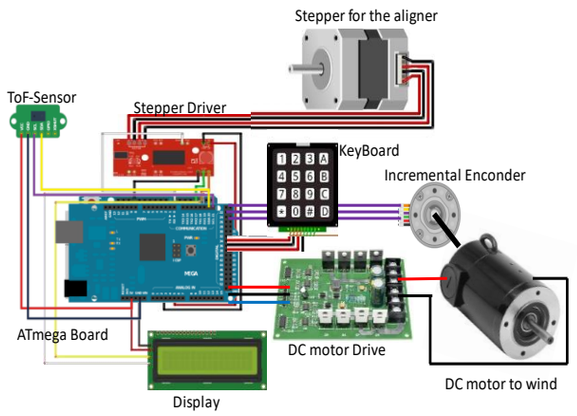

Figure 3 System stages

The complete equipment is presented in figure 4, where the system parts described previously are mounted on an aluminum mechanical structure. It was form with aluminum bosch framing, there exist a frame to support the optical fiber filament and is set on top of the structure. The position of that structure can be adjusted to stay in the middle of the spool, so this form is the aligning car moves in a specific gap.

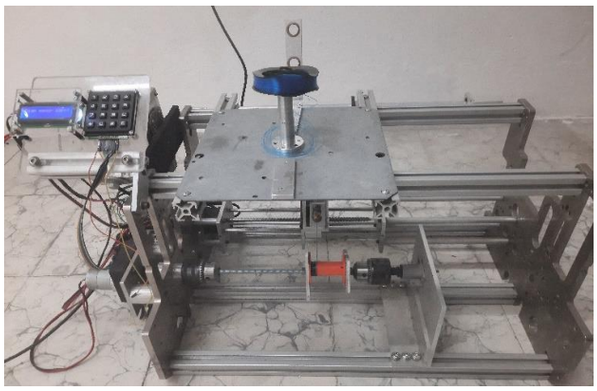

Figure 4 Real winding platform for optical fiber

Results

The moment when the system takes its time to calculate the number of layer and turs, allows the user to see if the winding can be conformed and the error is also calculated and validated with a specific length optical fiber filament, with a 100 meters filament. The extra material wounded around the spool was the 0.05 percent which was closed to the error estimated with the equation programmed in the microprocessor.

Conclusions

In conclusion, the system shows a low winding error, the use of fast development boards and the suitable mechanic platform allow a quick equipment construction, without a big budget and obtaining a good performance during its operation. Due to the modularity of the system, there are several future projects and opportunity areas, such as intelligent control algorithm, copper wire winding for transformer design using different gauge and vision control.

Acknowledgments

The authors acknowledge the financial support of the University of Guanajuato to publish this work 2022 and PRODEP support 2021. Authors also recognize the facilities and the support received by Autonomous University of Queretaro to accomplish this work in 2022.

References

Liwei Deng, Hongfei Suo and Haonan Ren (2021), Design of Insulation Tape Tension Control Systemof Transformer Winding Machine Based on Fuzzy PID, Sensors 2021, 21, 6512, https://doi.org/10.3390/s21196512.

ISSN 2524-2121

Campos, F. V. A. (2022). Las trabajadoras del hilo y la aguja. El oficio de las costureras a domicilio en la ciudad de Mexico durante las primeras decadas del siglo XX. Millars. Espai Història, Vol. LII 2022/1 pp. 41-75. http://dx.doi.org/10.6035/Millars

Ferrer-ALOS, L. The guild when interested. Production and commercialization of silk scarves in Manresa (Cataluna) in the 18th century. Continuity and Change (2020), Vol.35, pp. 53–74 doi:10.1017/S0268416020000090

Jia Ming, Yang Gongliu, Research of Optical Fiber Coil Winding Model Based on Large-deformation Theory of Elasticity and Its Application, Chinese Journal of Aeronautics Vol. 24, issue 5, (2011), pp. 640-647.

Pragnya Sanjiv Kanade and Someshwar S. Bhattacharya (2014), Designing a Cartridge Winder with Electronic Control, Journal of Engineered Fibers and Fabrics 9(2):112-119, doi:10.1177/155892501400900214.

Cabral Mosquera, F. N. (2022). Diseño de matriz por deformación progresiva para la fabricación de piezas de aluminio para dispositivos electromecánicos (Doctoral dissertation, Universidad Politécnica de Valencia).

Z Kang, S Li, X Li, D Xiu, B Guo (2020), Study on precise detecting and controlling technology of lag angle based on image processing, Journal of Physics Conference Series 1507(9):092002, doi:10.1088/1742-6596/1507/9/092002.

Zhonglin Guo, Jianhui Zhao and He Xu (2016), High-precision tension control method for starting and stopping of optical fiber winding based on trajectory planning, 5th International Conference on Environment, Materials, Chemistry and Power Electronics (EMCPE 2016).

Jiandong Chen, Tianying Chang, Qunjian Fu, Jinpeng Lang, Wenzhi Gao, Zhongmin Wang, Miao Yu, Yanbo Zhang and Hong-Liang Cui (2016), A Fiber-Optic Interferometric Tri-Component Geophone for Ocean Floor Seismic Monitoring, Sensors 2017, 17(1), 47, doi:10.3390/s17010047.

Yu. Korkishko, V.Fedorov, V.Prilutskii, V.Ponomarev, I.Morev, S.Kostritskii, A.Zuev, V.Varnakov (2012), Closed loop fiber optical gyroscopes for commercial and space applications, Conference: Inertial Sensors and Systems - Symposium Gyro Technology 2012.

Daisuke Tabuchi, Takao Sajima, Toshiro Doi, Hiromichi Onikura, Osamu Ohnishi, Syuhei Kurokawa and Takahiro Miura (2011), Development of a Filament-Winding Machine Based on Internal Heating by a High-Temperature Fluid for Composite Vessels, Sensors and Materials, Vol. 23, No. 6 (2011), pp. 347–358

Ferrer-Alos, L. El gremio cuando interesa: Produccion y comercializacion de panuelos de seda en Manresa (Cataluna) en el siglo XVIII. Studia Historica: Historia Moderna, 44(1), pp. 409-444.
https://doi.org/10.14201/shhmo2022441407442

[Title in Times New Roman and Bold No. 14 in English and Spanish]

Surname (IN UPPERCASE), Name 1st Author†*, Surname (IN UPPERCASE), Name 1st Co-author, Surname (IN UPPERCASE), Name 2nd Co-author and Surname (IN UPPERCASE), Name 3rd Co-author

Institutional Affiliation of Author including Dependency (No.10 Times New Roman and Italic)

International Identification of Science - Technology and Innovation

ID 1st Author: (ORC ID - Researcher ID Thomson, arXiv Author ID - PubMed Author ID - Open ID) and CVU 1st author: (Scholar-PNPC or SNI-CONACYT) (No.10 Times New Roman)

ID 1st Co-author: (ORC ID - Researcher ID Thomson, arXiv Author ID - PubMed Author ID - Open ID) and CVU 1st co-author: (Scholar or SNI) (No.10 Times New Roman)

ID 2nd Co-author: (ORC ID - Researcher ID Thomson, arXiv Author ID - PubMed Author ID - Open ID) and CVU 2nd co-author: (Scholar or SNI) (No.10 Times New Roman)

ID 3rd Co-author: (ORC ID - Researcher ID Thomson, arXiv Author ID - PubMed Author ID - Open ID) and CVU 3rd co-author: (Scholar or SNI) (No.10 Times New Roman)

(Report Submission Date: Month, Day, and Year); Accepted (Insert date of Acceptance: Use Only ECORFAN)

Abstract (In English, 150-200 words)

Objectives
Methodology
Contribution

Abstract (In Spanish, 150-200 words)

Objectives
Methodology
Contribution

Keywords (In English)

Indicate 3 keywords in Times New Roman and Bold No. 10

Keywords (In Spanish)

Indicate 3 keywords in Times New Roman and Bold No. 10

Citation: Surname (IN UPPERCASE), Name 1st Author, Surname (IN UPPERCASE), Name 1st Co-author, Surname (IN UPPERCASE), Name 2nd Co-author and Surname (IN UPPERCASE), Name 3rd Co-author. Paper Title. ECORFAN Journal-Taiwan. Year 1-1: 1-11 [Times New Roman No.10].

* Correspondence to Author (example@example.org)
† Researcher contributing as first author.

Introduction

Text in Times New Roman No.12, single space.

General explanation of the subject and explain why it is important.

What is your added value with respect to other techniques?

Clearly focus each of its features

Clearly explain the problem to be solved and the central hypothesis.

Explanation of sections Article.

Development of headings and subheadings of the article with subsequent numbers

[Title No.12 in Times New Roman, single spaced and bold]

Products in development No.12 Times New Roman, single spaced.

Including graphs, figures and tables-Editable

In the article content any graphic, table and figure should be editable formats that can change size, type and number of letter, for the purposes of edition, these must be high quality, not pixelated and should be noticeable even reducing image scale.

[Indicating the title at the bottom with No.10 and Times New Roman Bold]

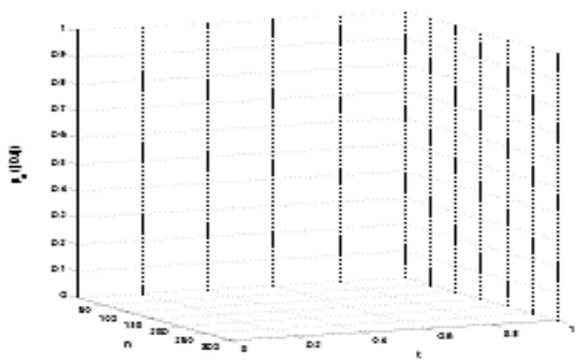

Graphic 1 Title and *Source (in italics)*

Should not be images-everything must be editable.

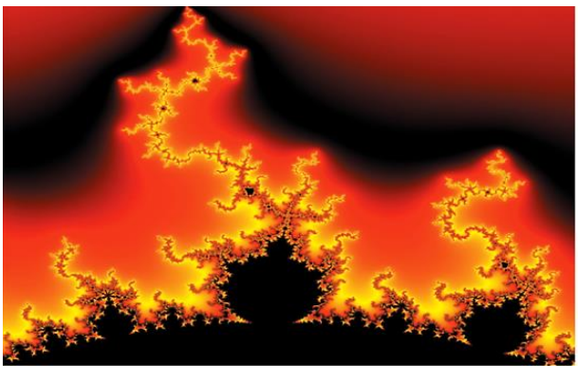

Figure 1 Title and *Source (in italics)*

Should not be images-everything must be editable.

Table 1 Title and *Source (in italics)*

Should not be images-everything must be editable.

Each article shall present separately in **3 folders**: a) Figures, b) Charts and c) Tables in .JPG format, indicating the number and sequential Bold Title.

For the use of equations, noted as follows:

$$Y_{ij} = \alpha + \sum_{h=1}^{r} \beta_h X_{hij} + u_j + e_{ij} \qquad (1)$$

Must be editable and number aligned on the right side.

Methodology

Develop give the meaning of the variables in linear writing and important is the comparison of the used criteria.

Results

The results shall be by section of the article.

Annexes

Tables and adequate sources

Thanks

Indicate if they were financed by any institution, University or company.

Conclusions

Explain clearly the results and possibilities of improvement.

ISSN 2524-2121

References

Use APA system. Should not be numbered, nor with bullets, however if necessary numbering will be because reference or mention is made somewhere in the Article.

Use Roman Alphabet, all references you have used must be in the Roman Alphabet, even if you have quoted an Article, book in any of the official languages of the United Nations (English, French, German, Chinese, Russian, Portuguese, Italian, Spanish, Arabic), you must write the reference in Roman script and not in any of the official languages.

Technical Specifications

Each article must submit your dates into a Word document (.docx):

Journal Name
Article title
Abstract
Keywords
Article sections, for example:

1. Introduction
2. Description of the method
3. Analysis from the regression demand curve
4. Results
5. Thanks
6. Conclusions
7. References

Author Name (s)
Email Correspondence to Author
References

Intellectual Property Requirements for editing:

- Authentic Signature in Color of Originality Format Author and Co-authors.

- Authentic Signature in Color of the Acceptance Format of Author and Co-authors.

- Authentic Signature in blue colour of the Conflict of Interest Format of Author and Co-authors.

ISSN 2524-2121

Reservation to Editorial Policy

ECORFAN Journal-Taiwan reserves the right to make editorial changes required to adapt the Articles to the Editorial Policy of the Journal. Once the Article is accepted in its final version, the Journal will send the author the proofs for review. ECORFAN® will only accept the correction of errata and errors or omissions arising from the editing process of the Journal, reserving in full the copyrights and content dissemination. No deletions, substitutions or additions that alter the formation of the Article will be accepted.

Code of Ethics - Good Practices and Declaration of Solution to Editorial Conflicts

Declaration of Originality and unpublished character of the Article, of Authors, on the obtaining of data and interpretation of results, Acknowledgments, Conflict of interests, Assignment of rights and Distribution.

The ECORFAN-Mexico, S.C Management claims to Authors of Articles that its content must be original, unpublished and of Scientific, Technological and Innovation content to be submitted for evaluation.

The Authors signing the Article must be the same that have contributed to its conception, realization and development, as well as obtaining the data, interpreting the results, drafting and reviewing it. The Corresponding Author of the proposed Article will request the form that follows.

Article title:

– The sending of an Article to ECORFAN Journal- Taiwan emanates the commitment of the author not to submit it simultaneously to the consideration of other series publications for it must complement the Format of Originality for its Article, unless it is rejected by the Arbitration Committee, it may be withdrawn.

– None of the data presented in this article has been plagiarized or invented. The original data are clearly distinguished from those already published. And it is known of the test in PLAGSCAN if a level of plagiarism is detected Positive will not proceed to arbitrate.

– References are cited on which the information contained in the Article is based, as well as theories and data from other previously published Articles.

– The authors sign the Format of Authorization for their Article to be disseminated by means that ECORFAN-Mexico, S.C. In its Holding Taiwan considers pertinent for disclosure and diffusion of its Article its Rights of Work.

– Consent has been obtained from those who have contributed unpublished data obtained through verbal or written communication, and such communication and Authorship are adequately identified.

– The Author and Co-Authors who sign this work have participated in its planning, design and execution, as well as in the interpretation of the results. They also critically reviewed the paper, approved its final version and agreed with its publication.

– No signature responsible for the work has been omitted and the criteria of Scientific Authorization are satisfied.

– The results of this Article have been interpreted objectively. Any results contrary to the point of view of those who sign are exposed and discussed in the Article.

Copyright and Access

The publication of this Article supposes the transfer of the copyright to ECORFAN-Mexico, SC in its Holding Taiwan for its ECORFAN Journal- Taiwan, which reserves the right to distribute on the Web the published version of the Article and the making available of the Article in This format supposes for its Authors the fulfilment of what is established in the Law of Science and Technology of the United Mexican States, regarding the obligation to allow access to the results of Scientific Research.

Article Title:

Name and Surnames of the Contact Author and the Co-authors	Signature
1.	
2.	
3.	
4.	

Principles of Ethics and Declaration of Solution to Editorial Conflicts

Editor Responsibilities

The Publisher undertakes to guarantee the confidentiality of the evaluation process, it may not disclose to the Arbitrators the identity of the Authors, nor may it reveal the identity of the Arbitrators at any time.

The Editor assumes the responsibility to properly inform the Author of the stage of the editorial process in which the text is sent, as well as the resolutions of Double-Blind Review. The Editor should evaluate manuscripts and their intellectual content without distinction of race, gender, sexual orientation, religious beliefs, ethnicity, nationality, or the political philosophy of the Authors.

The Editor and his editing team of ECORFAN® Holdings will not disclose any information about Articles submitted to anyone other than the corresponding Author.

The Editor should make fair and impartial decisions and ensure a fair Double-Blind Review.

Responsibilities of the Editorial Board

The description of the peer review processes is made known by the Editorial Board in order that the Authors know what the evaluation criteria are and will always be willing to justify any controversy in the evaluation process. In case of Plagiarism Detection to the Article the Committee notifies the Authors for Violation to the Right of Scientific, Technological and Innovation Authorization.

Responsibilities of the Arbitration Committee

The Arbitrators undertake to notify about any unethical conduct by the Authors and to indicate all the information that may be reason to reject the publication of the Articles. In addition, they must undertake to keep confidential information related to the Articles they evaluate.

Any manuscript received for your arbitration must be treated as confidential, should not be displayed or discussed with other experts, except with the permission of the Editor.

The Arbitrators must be conducted objectively, any personal criticism of the Author is inappropriate.

The Arbitrators must express their points of view with clarity and with valid arguments that contribute to the Scientific, Technological and Innovation of the Author.

The Arbitrators should not evaluate manuscripts in which they have conflicts of interest and have been notified to the Editor before submitting the Article for Double-Blind Review.

Responsibilities of the Authors

Authors must guarantee that their articles are the product of their original work and that the data has been obtained ethically.

Authors must ensure that they have not been previously published or that they are not considered in another serial publication.

Authors must strictly follow the rules for the publication of Defined Articles by the Editorial Board.

The authors have requested that the text in all its forms be an unethical editorial behavior and is unacceptable, consequently, any manuscript that incurs in plagiarism is eliminated and not considered for publication.

Authors should cite publications that have been influential in the nature of the Article submitted to arbitration.

Information services

Indexation - Bases and Repositories

RESEARCH GATE (Germany)
GOOGLE SCHOLAR (Citation indices-Google)
MENDELEY (Bibliographic References Manager)
HISPANA (Information and Bibliographic Orientation-Spain)

Publishing Services

Citation and Index Identification H
Management of Originality Format and Authorization
Testing Article with PLAGSCAN
Article Evaluation
Certificate of Double-Blind Review
Article Edition
Web layout
Indexing and Repository
ArticleTranslation
Article Publication
Certificate of Article
Service Billing

Editorial Policy and Management

69 Street. YongHe district, ZhongXin. Taipei-Taiwan. Phones: +52 1 55 6159 2296, +52 1 55 1260 0355, +52 1 55 6034 9181; Email: contact@ecorfan.org www.ecorfan.org

ECORFAN Journal-Taiwan

2524-2121
ISSN 2524-2121

www.ecorfan.org